Robust design of CAV-Dedicated lanes considering CAV demand uncertainty and lane reallocation policy

Seilabi, Sania E.; Pourgholamali, Mohammadhosein; Homem de Almeida Correia, Gonçalo; Labi, Samuel

DOI
10.1016/j.trd.2023.103827

Publication date
2023

Document Version
Final published version

Published in
Transportation Research Part D: Transport and Environment

Transportation Research Part D 121 (2023) 103827

Contents lists available at ScienceDirect

Transportation Research Part D

journal homepage: www.elsevier.com/locate/trd

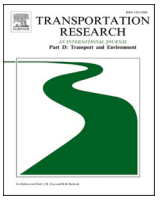

Robust design of CAV-Dedicated lanes considering CAV demand uncertainty and lane reallocation policy

Sania E. Seilabi [a,*], Mohammadhosein Pourgholamali [a], Gonçalo Homem de Almeida Correia [b], Samuel Labi [a]

[a] Lyles School of Civil Engineering, Purdue University, West Lafayette, IN 47907, USA
[b] Department of Transport & Planning TU Delft, 2600 GA Delft, the Netherlands

ARTICLE INFO

Keywords:
Connected and autonomous vehicles
Dedicated lanes
Lane reallocation policy
Traffic equilibrium
Robust optimization

ABSTRACT

Reduced headways of connected and automated vehicles (CAV) provide opportunities to address traffic congestion and environmental adversities. This benefit can be utilized by deploying CAV-dedicated lanes (CAVDL). This paper presents a bi-level optimization model that captures CAV market size uncertainty. The upper level determines the links (and number of lanes) for CAVDL deployment to minimize emissions. It considers lane reallocation policies that account for the prospect of smaller width of CAV-dedicated lane due to the smaller lateral wander of CAV tire tracks. This can increase the total number of lanes on wide highway sections. At the lower level, equilibrium and demand diffusion models capture travelers' route and vehicle-type choices. The bi-level model is formulated as a min–max mathematical program with equilibrium conditions and solved using the cutting-plane scheme and active-set algorithm. The computational experiments indicate that the robust plans have superior performance compared to the deterministic plan in pessimistic cases.

1. Introduction

Growing populations worldwide, particularly over the last century, continue to cause urban expansion and collateral problems of motorization, congestion, air quality degradation, and emissions. The notion of sustainability in urban development is receiving a great deal of attention (Jeon and Amekudzi, 2005; United Nations, 2018). To this end, emerging transportation technologies, particularly automated and connected transport systems, offer great promise in achieving efficient and safe mobility (Chang, 2019; Saeed et al., 2021), mitigating the related urban adversities, and ultimately promoting sustainable urban development (Federal Highway Administration, 2018; Ong and Hwang, 2019; Volpe Center, 2015).

The connectivity feature of connected and automated vehicles (CAVs) enables the exchange of information to/from other CAVs through V2V and intelligent roadside units. This allows CAVs to form platoons, which decreases headways and therefore increases road capacity, and decreases energy consumption (Le Hong and Zimmerman, 2021; Wang et al., 2022). There exist several studies that have investigated CAV platooning and its impacts on traffic mobility and emissions. For example, Li and Li (2022) proposed a docking strategy for CAVs that enables vehicles to dock on or split enroute to form platoon. This platooning strategy can improve mobility, riding comfort, and energy efficiency. The authors formulated the CAV docking and platooning question as a two-stage optimization

* Corresponding author.
E-mail address: sesmaei@purdue.edu (S.E. Seilabi).

https://doi.org/10.1016/j.trd.2023.103827
Received 2 September 2022; Received in revised form 12 May 2023; Accepted 19 June 2023
Available online 26 June 2023

problem and demonstrated that docking speed is a significant determinant of operations costs. Li and Yao (2022) compared different car-following models for CAV platoon trajectory advisory strategies. Their analysis demonstrated the significant benefits in terms of fuel efficiency, travel time and system cost by using Gipps' car-following model. Yao and Li (2020) proposed a decentralized control model for CAV platoon trajectory optimization to minimize travel time, fuel consumption, and safety risks of CAVs. Their analysis showed that decentralized control strategy can perform as well as centralized control strategies despite less technological maturity. Pribyl et al. (2020) and Wadud et al. (2016) also demonstrated the potential of CAVs for addressing vehicle emissions through platooning and energy consumption reduction.

Considering the platooning benefits, CAVs and CAV-related infrastructure can potentially help reduce congestion by managing travel demand and increasing the quantity and/or quality of travel supply. This is important, especially during a prospective era during which CAV deployment on public roads and their market penetration will grow. This era, referred to as the "transition period," is expected to be a long, drawn-out process spanning several years. During this period, CAVs and human-driven vehicles (HDVs) will share the roadways either directly as mixed traffic and/or through sharing of the roadway space via dedicated lanes. The concept of gradual, scheduled CAV-dedicated lane deployment enables metropolitan authorities to match supply (public investments in CAV infrastructure) to match demand (growing CAV market penetration). For any transportation initiative, while seeking to preserve the technical efficacy of the initiative, its wider impacts on the environment, economy, and social capital must be managed. In the case of infrastructure to support CAV operations, it is important to not only ensure the safety and mobility benefits of CAVs but also to ensure that they do not pose an undue burden on the economy (such as road user travel time cost), the environment (such as emissions), and society (such as equity across the two vehicle classes). Given the goal of increasing mobility, the literature focuses on lane dedication to CAVs while providing at least a lane for HDVs to reduce public opposition. It should be noted that all lanes are accessible to CAVs to provide flexibility in utilizing the road space. Similarly, in this research, lanes are divided into two groups, CAV-dedicated and general-purpose (GP) lanes, where GP lanes are accessible to both CAVs and HDVs.

This paper focuses on the subject of sustainable design of CAV-dedicated lanes in the prospective era of CAVs from the perspectives of all three key stakeholders. The objective of the paper is to develop an optimal network-wide plan for deploying CAV-dedicated lanes (in terms of the number of lanes to deploy and which year to deploy each of them) such that environmental impacts (vehicle emissions) are minimized, accounting for potential CAV market size uncertainty.

2. A review of the literature

Table 1 summarizes the literature associated with the CAV-dedicated lane deployment. From the review, it is observed that a number of researchers have highlighted the need to investigate CAV-dedicated lane planning using a variety of methods. Chen et al. (2016) investigated optimal deployment strategies for dedicated lanes during the CAV transition period to minimize social costs, including safety and total travel costs for HDVs and AVs. They divided the transition period into small (1-year) periods and established the CAV market penetration using a diffusion model (where the market penetration rate in a given period depends on that of the preceding period), and they compared the net benefits of CAVs and HDVs in terms of safety and travel time savings. Ye and Wang (2018) proposed the simultaneous design of traffic networks with the deployment of CAV lanes and congestion pricing to mitigate traffic congestion in the network. They showed that the integration of these planning strategies can outperform either CAV lane deployment alone or congestion pricing alone. Liu and Song (2019) developed a framework to identify the optimal road links to deploy CAV-dedicated lanes where HDV travelers are permitted to use these lanes by paying a toll. They demonstrated that by considering smaller headways for CAVs, the equilibrium flow may not be unique under mixed CAV and HDV flows. Wu et al. (2020) carried out the system-optimal design for a small network (with HDV streets and CAV expressways) under congestion pricing in a bid to minimize the cost of system travel time. Using a bi-level framework, Madadi et al. (2020) investigated the metropolitan authorities' decisions on road link retrofit by, for example, installing machine-readable road signs and lane markings to accommodate AVs. At the upper level, the total cost of link retrofit, and total system travel time were minimized, and at the lower level, travelers' route choice decisions were optimized using a logit-based stochastic user equilibrium model.

Table 1
Summary of literature review on CAV-dedicated lane deployment.

Study	Objective	Uncertainty (context)	Lane reallocation	Network (N)/Corridor (C) level
Chen et al. (2016)	Costs of safety and total travel time	No	No	N
Ye and Wang (2018)	Total travel time	No	No	N
Liu and Song (2019)	Total travel time	Yes (i.e., Equilibrium flow for a mixed fleet of CAV-HDVs)	No	N
Wu et al. (2020)	Total travel time and distance	No	No	N/C
Madadi et al. (2020)	Costs of network adjustment for CAVs and total travel time	No	No	N
Ghiasi et al. (2017)	Highway throughput	No	Yes	C
This paper	Worst-case total vehicle emissions	Yes (Potential market size of CAV)	Yes	N

Past studies analyzed the effect of narrow lanes on individual road corridors, or links, on road performance. To the best of our knowledge, the current study is the first to analyze the effect of narrow lanes on a road network. Doing this helps capture the holistic effects that characterize a connected road network: the change in lane width at one link affects the route choices of travelers and therefore affects the flow and travel times at not only that link but also at other links. In a hypothetical collection of separate and unconnected corridors (which does not constitute a network), the effect of reducing their lane widths is simply the sum of their individual effects. In such hypothetical scenario, the holistic effect is not applicable. On the other hand, for a road network of several corridor links, as in this paper, the effect of the sum of reduced lane widths is the holistic outcome, as this is different from the sum of the effects in the unconnected scenario. We capture this holistic effect using the traffic assignment (user equilibrium) model formulation. Currently, the standard lane width for highways in the United States is 12 ft. Due to the little or no lateral wander of CAVs (Ghiasi et al., 2020), CAV-dedicated lanes may have smaller lane widths from an HDV-only scenario to a mixed-stream scenario, and therefore, the number of lanes in a wide highway corridor can potentially be increased. The CAV-dedicated lane width could be close to the maximum vehicle width to accommodate more lanes (Dennis et al., 2017). For example, the width of the Tesla Model Y with unfolded mirrors is approximately 7 ft. Ghiasi et al. (2020) proposed a lane reallocation policy for a highway corridor to identify the optimal number of reduced-width CAV-dedicated lanes to maximize the highway segment throughput. In contrast to the network-level context of our study, Ghiasi et al. (2020) capture the possibility of reducing the lane width to possibly increase the number of lanes on a single highway corridor.

The uncertainty in HDV and CAV travel demand forecasts is inevitable over the long-term planning horizon. This can stem from two main reasons. The first is the uncertainty of travel demand over a long planning horizon due to changes in economic and demographic conditions over several years. The second is the uncertainty in the potential CAV market size, which is the variation in ownership of CAVs at a given point in time. This variation is due to the uncertainty in consumers' willingness to purchase a CAV, which in turn is due to the availability of transportation infrastructure such as charging stations and CAV-dedicated lanes, as well as consumer experience related to CAVs. The potential market size can be estimated using customer surveys (Gkartzonikas and Gkritza, 2019). In other words, the technological advancements and uncertainty in consumers' perceptions of these new technologies can cause uncertainty in the forecasting of the potential CAV market size. The potential CAV market size directly impacts the CAV travel demand, which is captured in this study by using the demand diffusion model. The diffusion model has been used in the context of transportation to obtain the travel demand for hydrogen-fueled vehicles (Park et al., 2011) and CAVs (Lavasani et al., 2016). Chen et al. (2016) captured the impact of CAV travel cost reduction due to lane deployment policy on CAV travel demand using the demand diffusion model. In the current paper, we focus on the design of CAV-dedicated lanes by capturing the potential CAV market size uncertainty.

Few studies in the literature capture the effects of the uncertainty of different parameters, such as vehicle purchase price, on the CAV-dedicated lane deployment. Chen et al. (2019) developed a two-stage stochastic programming model that considered uncertainty in the CAV purchase price. Liu and Song (2019) showed that the equilibrium flow may not be unique under a mixed flow of CAVs and HDVs, considering the impact of mixed flow on road capacity. The authors proposed a robust optimization program to minimize the maximum travel time under different equilibrium flows. However, none of these studies captured the uncertainty in consumers' responses to purchasing CAVs and, consequently, the potential CAV market size over several years. In the current paper, we address the uncertainty in the potential CAV market size, which is related to the uncertainty in CAV travel demand. In the analysis, we assume that

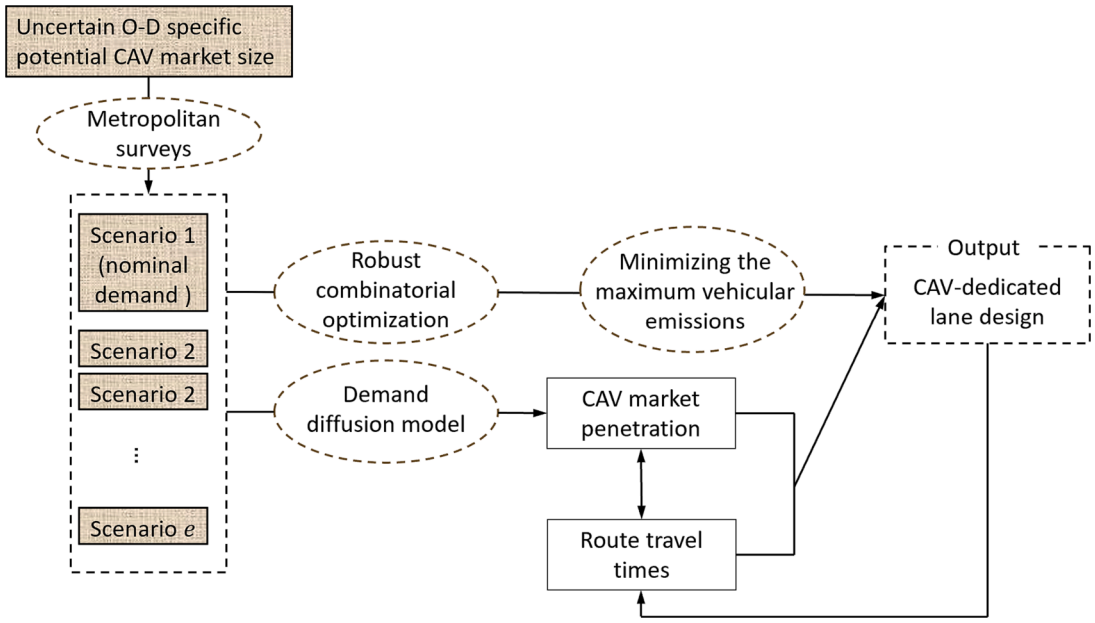

Fig. 1. Impact of potential CAV market size uncertainty in CAV-dedicated lane design.

the aggregate travel demand of HDVs and CAVs is known and therefore do not consider the uncertainty in travel demand forecasts over several years.

To address the potential CAV market size uncertainty, we developed a robust planning framework for CAV-dedicated lane deployment. This framework assumes that the potential CAV market size can be one of the scenarios in an uncertainty set with unknown probability distribution. This will help accommodate in the analysis, any variations of the CAV market size. The possible values in this set can be identified based on forecasts by the metropolitan authorities (Bertsimas and Sim, 2003; Lou et al., 2009). The robust model minimizes the total emissions costs relative to the worst-case scenario. It is formulated as a bi-level problem where the upper level captures the decision of metropolitan authorities who aim to minimize the maximum total emissions costs under different scenarios of potential CAV market size. The decision to deploy CAV-dedicated lanes is subject to the total road width available. Allocating reduced lane widths to CAVs will generally result in increased capacity available to CAVs, fewer interactions with HDVs, and higher travel time reliability. These will make CAV-dedicated lanes more attractive to travelers and therefore encourage consumers to purchase CAVs, which is consistent with the goal of vehicle emissions minimization. The CAV-dedicated lanes, given reduced headways and therefore increased capacity available to CAVs, can reduce the travel time, which encourages the travelers to adopt CAVs (Shabanpour et al., 2018, 2017). The upper-level model is formulated as a mixed-integer nonlinear program. The potential CAV market size is assumed to be origin–destination (O-D) specific to provide flexibility for transportation decision-makers in capturing the variation in CAV affordability for travelers from different regions. Fig. 1 summarizes the interaction between potential CAV market size uncertainty, network travel times, and CAV-dedicated lane design.

Table 2
List of notations.

Sets	
O	Set of nodes
A	Set of links
T	Set of the periods
W	Set of O-D pairs
$\overline{A}$	Set of candidate links for CAV-dedicated lanes
$\overline{\overline{A}}$	Set of candidate links for lanes reduction
H	Set of CAV-dedicated link pair candidates
N	Set of vehicle types
Q	Network-level CAV market size uncertainty set
K_w^t	O-D pair CAV market size uncertainty scenario of O-D pair $w \in W$ in period t
Parameter	
ϕ_a	per-lane per-hour capacity of link a
$J_{\overline{a}}$	Maximum number of lane increase for links $\overline{a}$
α_n	Value of time of travelers using vehicle type n
χ_w^t	The annual trip number of O-D pair w in period t
ξ_w^t	CAV additional cost of O-D pair w in period t
u_a	Per-lane width of link a (ft. or meters)
Δ	Node-link incidence matrix
τ_a^0	Free-flow travel time of link a
κ	Monetized factor of emissions ($/kg)
$\widehat{q}_w^{t,k}$	Potential CAV market size of O-D pair w, in time period t, in uncertainty set k
Λ^t	Uncertainty budget at period t
ε	A sufficiently small number
φ	Parameter of diffusion model
ι	Parameter of diffusion model
$\boldsymbol{E}_w^n$	Origin and destination set of O-D pair w of travel class n
d_a	Length of link a
ψ^t	Share of E-HDVs in time period t
$\theta_a^{n,t}$	Extra travel cost for travel class n in period t due to the lack of CAV-dedicated lane on link a
Variables	
$q_w^{n,t}$	Travel demand of class n of O-D pair w in period t
$c_w^{n,t}$	Equilibrium travel time of vehicle type n of O-D pair w in period t
μ_w^t	Benefits gained by CAV travelers of O-D pair w in period t due to CAV-dedicated lane deployment
$\overline{q}_w^t$	Potential CAV market size for O-D pair w in period t
g_w^t	Intrinsic growth factor of O-D pair w at period t
τ_a^t	Travel time of link a in period t
e_a^t	Vehicle emissions of HDV travelers using link a in period t
ζ_a^t	Capacity of link a in period t
TEC	Total vehicle emissions cost
$p_w^{t,k}$	Binary variable that is equal to 1 if scenario k is realized for O-D pair w in period t
$\pi_{i,w}^{n,t}$	Equilibrium travel time of travelers of class n traveling between O-D pair w when reaching node i in period t
$y_{\overline{a}}^t$	Number of deployed CAV-dedicated lanes on link $\overline{a}$ in period t
$y_{\overline{\overline{a}}}^t$	Number of converted lanes on link $\overline{a}$ in period t
$x_{a,w}^{n,t}$	Traffic flow of vehicle type n at link a, between O-D pair w in period t
ν_a^t	Aggregate flow of all vehicle types and O-D pairs at link a in period t

The lower-level decision aims to capture the vehicle type, route, and lane choices of travelers. The GP lanes can be used by both HDV and CAV travelers, whereas CAV-dedicated lanes can be used by only CAV travelers. The values of time for two classes of travelers, CAV and HDV travelers, are assumed to be different. However, travelers within each class are assumed to have the same value of time. Since the bi-level model contains integer variables and nonlinear constraints, it is classified as a non-polynomial (NP)-hard problem and is difficult to solve. Hence, we adopt the cutting-plane scheme to solve the problem.

The contributions of this study are threefold. First, this study develops a method for CAV-dedicated lane management considering, unlike most past studies, the uncertainty in the potential CAV market size over several years. This study explores the interaction between the impacts of uncertainty in the potential CAV market size on the CAV-dedicated lane deployment design at different CAV market penetrations. Secondly, the study captures the fact that CAVs require a smaller lane width compared to HDVs, and therefore, for wide existing corridors, metropolitan authorities can increase the number of road lanes within the overall roadway cross-section. Thirdly, the context of the study is the deployment of CAV-dedicated lanes to minimize environmental (vehicle emissions) costs. Environmental impacts can have long-term consequences for the sustainability of a city. One example of an agency considering emission reduction is the USDOT's Congestion Mitigation and Air Quality Improvement (CMAQ) program which provides funds to states for transportation projects designed to reduce traffic congestion and improve air quality (USDOT Center for Climate Change, 2017). Another example is the Carbon Reduction Program (CRP) that helps states develop carbon reduction strategies and address the climate crisis in the US (Federal Highway Administration, 2022). The urban vehicular emissions minimization goal is the focus of several studies in the context of transportation network design and management for HDVs only (Ma et al., 2017, 2015; Miralinaghi, 2018; Miralinaghi and Peeta, 2020, 2019; Xu et al., 2015; Yang et al., 2017, 2014; Pourgholamali et al., 2023). Metropolitan authorities must consider the environmental impacts of their decisions to ensure the health and well-being of citizens. By considering environmental impacts, metropolitan authorities can demonstrate their commitment to the values and priorities of their citizens.

The remaining sections are structured as follows: Sections 2 and 3 provide the preliminaries and methodology. Section 4 briefly discusses the solution algorithm, followed by numerical experiments that compare the performance of robust and deterministic designs of CAV-dedicated lanes in Section 5. Finally, Section 6 provides the study insights and concluding remarks. The used notations throughout the paper are summarized in Table 2.

3. Preliminaries

The road transportation network can be represented by the graph $G = (O, A)$ where O and A are the sets of nodes and directed links, respectively. The planning horizon, with a duration of several years, is divided into T periods where each period is denoted by $t \in \mathrm{T}$ and comprises a few years. The set of O-D pairs is denoted by W. The sets of candidate links for lane reduction and CAV-dedicated links are denoted by $\overline{\overline{A}}$ and $\overline{A}$. Consistent with previous research on CAV-dedicated lane deployment (Chen et al., 2016; Liu and Song, 2019), the set of CAV-dedicated link pair candidates is indexed by $H = [\overline{\overline{a}}, \overline{a}]$ where $\overline{\overline{a}} \in \overline{\overline{A}}$ and $\overline{a} \in \overline{A}$. This pair is constructed upon removing the first lane from link a. Then, during the planning horizon, lanes can be removed from $\overline{\overline{a}}$ and allocated to $\overline{a}$. For example, consider the four-node network in Fig. 2(a) where link numbers are shown on node connectors. If link 3 is a candidate for CAV-dedicated lane deployment, then the network is transformed into Fig. 2(b) where $A = \{1, 2, 3, 4\}$, $\overline{A} = \{5\}$, $\overline{\overline{A}} = \{3\}$ and $H = \{[3, 5]\}$. This transformation is due to the different capacities of CAV and GP lanes. After this transformation, link 3 (referred to as general purpose (GP) link) only consists of GP lanes and remains a candidate link for CAV-dedicated lanes. Link 5 is a link with only CAV-dedicated lanes (referred to as "CAV-dedicated link"). Let u_a and y_a^t denote the width and number of converted (or reduced) lanes on link $\overline{a} \in \overline{A}$ (or link $\overline{\overline{a}} \in \overline{\overline{A}}$). Further, ϕ_a denotes the per-lane per-hour capacity of link a. Let $J_{\overline{a}}$ and $J_{\overline{\overline{a}}}$ denote the maximum increased and reduced number of lanes for links $\overline{a}$ and $\overline{\overline{a}}$, respectively.

The mixed-traffic scenario consists of CAVs and HDVs, where N denotes the set of vehicle types. Let classes 1, 2 and 3 denote internal combustion engine HDVs (ICE-HDVs), electric HDVs (E-HDVs) and CAVs, respectively. Let $q_w^{n,t}$ denote the travel demand of class $n \in N$ of O-D pair $w \in W$ in period $t \in T$. The equilibrium travel time of vehicle type n of O-D pair w in period t is denoted by $c_w^{n,t}$. The equilibrium travel time of all HDVs is equal and therefore denoted by $c_w^{1,t}$. Let μ_w^t denote the benefits gained by CAV travelers of O-D pair w in period t due to CAV-dedicated lane deployment. A demand diffusion model is used in our study to capture the CAV travel

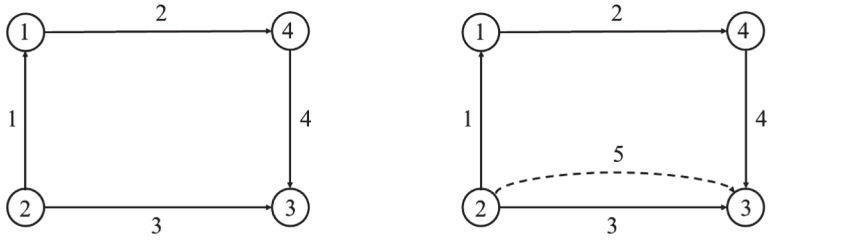

(a) Original network (b) Transformed network with CAV-dedicated link 5

Fig. 2. A four-node network for illustration purposes.

demand as follows:

$$q_w^{3,t} = q_w^{3,t-1} \bullet \left(1 + g\left(\mu_w^t\right) \bullet \left(1 - \frac{q_w^{3,t-1}}{\overline{q}_w^t}\right)\right) \forall w \in W, \forall t > 1 \tag{1}$$

$$g\left(\mu_w^t\right) = \varphi \bullet e^{\iota \bullet \left(\mu_w^t - \overline{\mu}_w^t\right)} \forall w \in W, \forall t \in T \tag{2}$$

$$\mu_w^t = \chi_w^t \bullet \left[\alpha_1 \bullet c_w^{1,t} - \alpha_2 \bullet c_w^{3,t}\right] - \xi_w^t \forall w \in W, \forall t \in T \tag{3}$$

$$q_w^t = \sum_{n=1}^{N} q_w^{n,t} \forall w \in W, \forall t \in T \tag{4}$$

$$q_w^{2,t} = \psi^t \left(q_w^t - q_w^{3,t}\right) \forall w \in W, \forall t \in T \tag{5}$$

$$q_w^{1,t} = \left(1 - \psi^t\right)\left(q_w^t - q_w^{3,t}\right) \forall w \in W, \forall t \in T \tag{6}$$

Equations (1) state that the CAV travel demand of each O-D pair in each period ($q_w^{3,t}$) depends on the demand on the previous period ($q_w^{3,t-1}$), the potential CAV market size ($\overline{q}_w^t$) and the gained benefits of that O-D pair (μ_w^t). Equations (2) denote the intrinsic growth coefficient of O-D pair $w \in W$ where φ and ι are positive constants and $\overline{\mu}_w^t$ denotes the O-D specific benefit threshold. Equations (3) calculate the benefits gained by O-D pair w in period t where α_n, χ_w^t and ξ_w^t are the value of time of class n, the number of trips, and CAV additional cost of O-D pair w in period t respectively. The value of time of E-HDVs and ICE-HDVs are assumed to be the equal to α_1. The additional cost can be due to the higher purchase price or operational costs. We are assuming that these are essentially commuter trips that need to be repeated frequently therefore affecting the attractiveness of adopting a certain type of vehicle. Equations (4)-(6) state the O-D pair travel demand for each vehicle class in time period t, where ψ^t is the share of E-HDVs in time period t.

Let $x_{a,w}^{n,t}$ denote the flow of link $a \in A$ between O-D pair w using vehicle type n in period t where $\boldsymbol{x}_w^{n,t}$ represents the vector of link flows for all links. Let ν_a^t denote the aggregate flow of link a in period t while $\boldsymbol{\nu}$ represents the vector of aggregate flows. For a given travel demand vector $\boldsymbol{q}$ across different O-D pairs, vehicle types and time periods, $V(\boldsymbol{q})$ shows the set of feasible link flows, as follows:

$$V(\boldsymbol{q}) = \left\{ \boldsymbol{\nu} | \boldsymbol{\nu} = \sum_{(w,n)} \boldsymbol{x}_w^{n,t}, \Delta \boldsymbol{x}_w^{n,t} = \boldsymbol{E}_w^n q_w^{n,t}, \boldsymbol{x}_w^{n,t} \geq 0, \forall w \in W, \forall n \in N, \forall t \in T \right\} \tag{7}$$

where $\boldsymbol{E}_w^n$ is an input–output vector of length $|O|$ (representing origin and destination for O-D pair $w \in W$) and Δ is the node-link incidence matrix associated with the given network. There exist two non-zero components in vector $\boldsymbol{E}_w^n$, (i) 1 for the origin node of O-D pair w and (ii) –1 for the destination node of O-D pair w. In the node-link incidence matrix Δ, there exist two non-zero components, (i) 1 for the starting node, and (ii) -1 for the ending node. Let τ_a^t denote the travel time of link a in period t which is a monotonically increasing function of link flow ν_a^t. In this study, it is assumed to follow the well-known Bureau of Public Roads (BPR) function:

$$\tau_a^t\left(\nu_a^t, c_a^t\right) = \tau_a^0 \bullet \left(1 + 0.15\left(\frac{\nu_a^t}{\zeta_a^t}\right)^4\right) \forall a \in A, \ \forall t \in T \tag{8}$$

where τ_a^0 and ζ_a^t denote the free-flow travel time and capacity of link a. The vehicle emissions function of HDV travelers using link a in period t is denoted by e_a^t, that is assumed to be nonnegative and monotonically increasing as a function of ν_a^t. For three reasons, carbon monoxide (CO) is used as a proxy for vehicle emissions in this study. First, among different vehicle emissions types, CO is a major pollutant (Xu et al., 2015). Second, the CO emissions function is similar to that for other pollutants. Let d_a and τ_a^t denote the length (in km) and travel time (in min) of link a in period t, respectively. The CO emissions function (in g/veh) of ICEVs using link a in period t is formulated by Wallace et al. (1998) and used by several studies (Ma et al., 2017, 2015; Xu et al., 2015; Yang et al., 2017, 2014) as follows:

$$e_a^t\left(\nu_a^t\right) = 0.2038\tau_a^t\left(\nu_a^t, c_a^t\right) \bullet exp\left(\frac{0.7962 d_a}{\tau_a^t\left(\nu_a^t, c_a^t\right)}\right) \forall a, \forall t \tag{9}$$

We assume that CAVs are electric and generate zero local emissions. There are multiple reasons why, in the future, most CAVs will be electric. First, EVs are more energy efficient than ICEVs (Jorgensen, 2008). Since CAVs are likely to be operated for long periods, particularly without a driver, it seems intuitive to use an energy-efficient power source. Second, EVs can offer instant torque, which means they can accelerate quickly and smoothly, which is a desirable feature for CAVs that drive closer to each other (Das and Sharma, 2022). Third, there is already a growing infrastructure of charging stations for EVs. This makes it increasingly attractive for users to own and operate electric CAVs. Fourth, EVs produce zero emissions at the point of use and generally lower net emissions over their life cycles (even where cradle-to-grave impacts are considered), which means that they can help reduce air pollution in cities (Ajanovic and Haas, 2016; Dunn et al., 2012; Hendrickson et al., 2006; Li et al., 2015; Peters et al., 2020). This is particularly important for CAVs, which are predicted to operate as ride-share vehicles primarily in urban environments where air quality is a concern. Several CAV manufacturers have announced plans to ensure that the vehicles they produce will use electricity as the power source. These include

General Motors, Waymo, Apple, and Tesla (General Motors, 2022; Gurman, 2021; Tesla, 2021; Valdes-Dapena, 2018). Hence, the internal combustion engine HDVs (ICE-HDVs) are assumed to be the only source of local emissions in the network. Let κ denote the monetized unit of vehicle emissions. The total vehicle emissions cost (*TEC*) can be formulated as follows:

$$TEC = \sum_{t}\sum_{(a,w)} \kappa e_a^t\left(v_a^t\right) x_{a,w}^{1,t} \tag{10}$$

4. Methodology

This section presents the bi-level framework for the robust optimization of CAV-dedicated lane deployment, considering the possible reduction of the lane width and a subsequent increase in the number of total lanes on a link. The bi-level framework is consistent with the Stackelberg structure and consists of an upper-level and a lower-level model. The upper-level model captures the goal of the metropolitan authority, which is assumed in this paper to be the minimization of the maximum emissions cost under all possible CAV market sizes over the long-term planning horizon. The decision for the metropolitan authority is to identify the number of lanes converted to CAVLS and reduction of the number of GP lanes. The lower-level model captures the route and vehicle type choices of travelers. Fig. 3 presents the structure of the bi-level framework.

It is difficult to reliably forecast the potential CAV market size due to current lack of CAV experience among travelers; therefore, this variable has significant uncertainty. To describe the uncertainty in the potential CAV market size we use a robust optimization approach that assumes that the potential CAV market size belongs to an uncertainty set (Bertsimas and Sim, 2003). To formulate the potential CAV market size uncertainty set, let $\hat{q}_w^{t,k}$, $k = 1, 2, \cdots K_w^t$ represent the potential CAV market size for O-D pair w in period t under scenario k. The first value in this set ($\hat{q}_w^{t,1}$), is assumed to be the predicted or nominal potential CAV market size. Let $p_w^{t,k}$ denote the binary variable that is equal to 1 if scenario k is realized for O-D pair w in period t, which is the worst-case scenario. There exists only one realized potential CAV market size for each vehicle type n between O-D pair w in period t, $\sum_{k\in K_w^t} p_w^{t,k} = 1$. Let Λ^t denote the uncertainty budget in period t where it implies that $\sum_w \sum_{k=2}^{|K|} p_w^{t,k} \le \Lambda^t$. A high uncertainty budget increases the number of possible potential CAV market size scenarios which leads to a higher computational burden but higher accuracy in deriving the robust design. It also reflects the risk-taking attitude of metropolitan authorities where the high-uncertainty budget implies the risk-aversion attitude of metropolitan authorities against several possible outcomes of future travel demand. Given these notations, the network-level potential CAV market size uncertainty set Q can be formulated as follows:

$$Q = \left\{ \overline{\boldsymbol{q}} \left| \sum_{k\in K_w^t} \hat{q}_w^{t,k} p_w^{t,k} = \overline{q}_w^t, \sum_{k\in K_w^t} p_w^{t,k} = 1, \sum_{(w)}\sum_{k=2}^{|K|} p_w^{t,k} \le \Lambda^t, p_w^{t,k} \in \{0,1\}, \forall t \in T \right. \right\} \tag{11}$$

where $\overline{\boldsymbol{q}} = (\hat{q}_w^{t,k}, \forall w \in W, k \in K_w^t, \forall t \in T)$. Let $\pi_{i,w}^{n,t}$ denote the equilibrium travel time of travelers of class n between O-D pair w at node i in period t. This bi-level program is formulated as a mathematical program with equilibrium conditions (MPEC1) as follows:

$$\min_{y} \max_{x,p} \sum_{t}\sum_{(a,w)} \kappa e_a^t\left(v_a^t\right) x_{a,w}^{1,t} \tag{12}$$

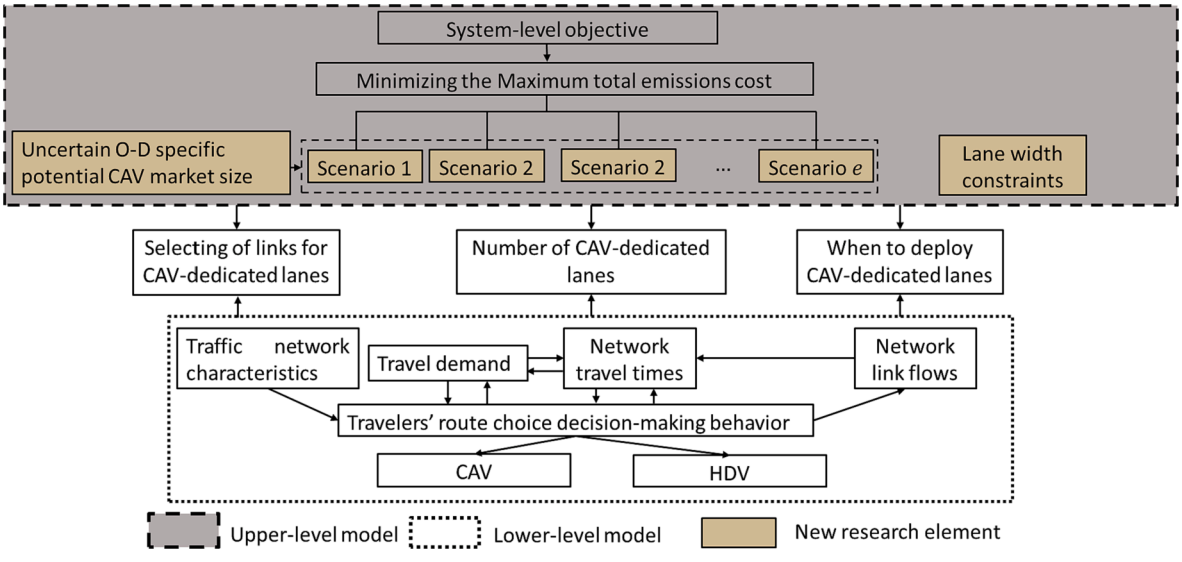

Fig. 3. Bi-level framework for CAV-dedicated lane deployment.

$$\zeta_{\overline{a}}^{t} = \zeta_{\overline{a}}^{t-1} + \phi_{\overline{a}} y_{\overline{a}}^{t} \; \forall \overline{a} \in \overline{A}, \forall t > 1 \tag{13}$$

$$\zeta_{\underline{\overline{a}}}^{t} = \zeta_{\underline{\overline{a}}}^{t-1} - \phi_{\underline{\overline{a}}} y_{\underline{\overline{a}}}^{t} \; \forall \underline{\overline{a}} \in \underline{\overline{A}}, \forall t > 1 \tag{14}$$

$$u_{\overline{a}} \bullet \left(\sum_{i=1}^{t} y_{\overline{a}}^{i} \right) \leq u_{\underline{\overline{a}}} \bullet \left(\sum_{i=1}^{t} y_{\underline{\overline{a}}}^{i} \right) \forall t \in T, \; \forall [\underline{\overline{a}}, \overline{a}] \in H \tag{15}$$

$$\zeta_{\underline{\overline{a}}}^{t} \geq \underline{\zeta}_{\underline{\overline{a}}} \forall \underline{\overline{a}} \in \underline{\overline{A}}, \; \forall t \in T \tag{16}$$

$$y_{\underline{\overline{a}}}^{t} \in \left\{ 0, \cdots, J_{\underline{\overline{a}}}^{t} \right\} \forall \underline{\overline{a}} \in \underline{\overline{A}}, \; \forall t \in T \tag{17}$$

$$y_{\overline{a}}^{t} \in \left\{ 0, \cdots, J_{\overline{a}}^{t} \right\} \forall \overline{a} \in \overline{A} \tag{18}$$

$$0 \leq x_{a,w}^{n,t} \perp \left(\tau_{a}^{t}\left(\nu_{a}^{t}, \zeta_{a}^{t} \right) + \pi_{i,w}^{n,t} - \pi_{j,w}^{n,t} \right) \geq 0 \, \forall n \in N, \forall w \in W, \forall t \in T, \; \forall (i,j) = a \in A \backslash \overline{A} \tag{19}$$

$$0 \leq x_{a,w}^{n,t} \perp \left(\tau_{\overline{a}}^{t}\left(\nu_{\overline{a}}^{t}, \zeta_{\overline{a}}^{t} \right) + \pi_{i,w}^{n,t} - \pi_{j,w}^{n,t} - \theta_{\overline{a}}^{n,t} \right) \geq 0 \, \forall n \in N, \forall w \in W, \forall t, \; \forall (i,j) = \overline{a} \in \overline{A} \tag{20}$$

$$x_{\overline{a},w}^{n,t} = 0 \, \forall n \in \{1,2\}, \; \forall w \in W, \forall t, \forall \overline{a} \in \overline{A} \tag{21}$$

$$x_{\overline{a},w}^{3,t} \leq M \bullet \sum_{i=1}^{t} y_{\overline{a}}^{i} \, \forall w \in W, \forall t \in T, \forall \overline{a} \in \overline{A} \tag{22}$$

$$x_{\overline{a},w}^{n,t} \bullet \theta_{\overline{a}}^{n,t} = 0 \, \forall w \in W, \forall n \in N, \forall t \in T, \; \forall \overline{a} \in \overline{A} \tag{23}$$

$$\theta_{\overline{a}}^{n,t} \geq 0 \, \forall n \in N, \forall t \in T, \forall \overline{a} \in \overline{A} \tag{24}$$

$$\nu \in V(q) \tag{25}$$

$$\boldsymbol{q} \in Q \tag{26}$$

(1)-(7), (11).

where θ captures the extra costs of HDV travelers due to the lack of ability to use CAV-dedicated lanes. Since CAV travelers can use CAV-dedicated lanes, this value can be only positive for HDV travelers. The upper-level model consists of equations (12)-(18). The goal of metropolitan authorities is to minimize the worst-case total emissions cost that can be realized under all possible scenarios for potential CAV market sizes. Constraints (13) state that the capacity of CAV-dedicated link $\overline{a}$ in period t is equal to the sum of capacity of that link in period $t-1$ and additional converted capacity of CAV-dedicated lane(s) in period t. Constraints (14) state that the capacity of GP link $\underline{\overline{a}}$ in period t can be derived by the deduction of capacity of converted lanes in period t from the capacity of that link in period $t-1$. Constraints (15) ensure that, considering the lane reallocation strategy, the total width of CAV-dedicated lanes and GP lanes for each link does not exceed its width. Constraints (16) ensure that there is a minimum road capacity for HDVs after lane reduction for each link in each period t. Constraints (17)-(18) describe the integer variables for the number of lanes increase and reduction on links $\overline{a}$ and $\underline{\overline{a}}$.

The lower-level model comprises equations (19)-(26), where the perpendicular operator $0 \leq A \perp B \geq 0$ means that $A \bullet B = 0, A \geq 0$, and $B \geq 0$. Equilibrium conditions (19)-(20) describe the route choice of travelers. Travelers alter their routes to reduce travel times unless they are unable to reduce them further by unilaterally altering the routes. Constraints (19) state the equilibrium conditions for the links, excluding those that are candidates for CAV-dedicated lanes. Constraints (20) state the equilibrium conditions for candidate links for CAV-dedicated lanes. It means that travelers of class n between O-D pair w use link a if this link is part of the shortest path between O-D pair w. Constraints (21) ensure that HDVs do not use CAV-dedicated links. Constraints (22) ensure that CAVs use CAV-dedicated links if some GP lanes are converted to CAV-dedicated lanes. Constraints (23)-(24) impose additional costs θ on vehicles traversing link a which is not feasible due to a lack of permission to use the CAV-dedicated links for HDV travelers. Constraints (25) denote travel demand conservation constraints. Constraints (26) describe the uncertainty set for potential CAV market size. As a result, MPEC1 ((1)-(9), (11)-(26)) is a nonlinear mathematical program with integer variables and can be classified as an NP-hard problem (Bazaraa et al., 2013). Given the difficulty of solving this class of mathematical programs, the active-set algorithm (Lou et al., 2009) is adopted and used to solve the problem as explained in the next section.

5. Solution algorithm

There exist several techniques to solve MPEC1 ((1)-(9), (11)-(26)), such as nonsmooth penalization (Scholtes and Stöhr, 1999), and directly relaxing complementarity constraints and solving MPCC as nonlinear programs (Raghunathan and Biegler, 2012). The cutting-plane scheme is used in this research. This scheme, first proposed by Lou et al. (2009) to solve a robust discrete network design

problem, solves a relaxed MPEC1 based on a definite set of potential CAV market sizes (set Q). To solve MPEC1 by implementing the cutting-plane scheme, two sub-problems must be defined: (i) MPEC2 is a relaxed MPEC1 and determines an optimal CAV-dedicated lane deployment plan, based on a set of generated cuts, (ii) WPS generates new cuts which are worst-case potential CAV market size sets leading to higher levels of total emissions cost, based on a CAV-dedicated lane deployment. The defined sub-problems are described in Appendix 1. The two subproblems are solved iteratively to find the optimal solution to MPEC1. In MPEC2, we transformed the integer decision variables (y_a^t) to binary ones. As the decision variables have integer values, the expression $y_a^t = \sum_{\varrho=1}^{\Phi_a^t} 2^{\varrho-1} \times z_{a,\varrho}^t$ is used, where $z_{a,\varrho}^t$ is binary and Φ_a^t is the largest integer that $J_a^t \leq 2^{\Phi_a^t} - 1$. This transformation to binary variables enables us to solve the problem using active-set algorithm later in this section. All of the defined constraint to MPEC2 has similar concept to those of MPEC1.

The overall iterative solution algorithm of MECP1 is shown in Algorithm 1. In this solution algorithm, WPS and MPEC2 are solved iteratively and provide each other's cut set and optimal CAV-dedicated lane deployment plan, respectively.

Algorithm 1.. (*Overall solution procedure.*)

1:	***Initializing***: *set* $\hat{z}_{a,\varrho}^t = 0$, $Q = \{\}$, *and counter* $= 0$ (***A0***)
2:	***Repeat***
3:	*Solve WPS based on* $\hat{z}_{a,\varrho}^t$ *and store the optimal solution in* $\hat{p}_w^{t,k}$ (***W0-W7***)
4:	*Update* $Q: Q = \hat{p}_w^{t,k} \cup Q$ (***A1***)
5:	*Solve MPEC2 based on Q and store the optimal solution in* $\hat{z}_{a,\varrho}^t$ (***M0-M7***)*counter* $\leftarrow$ *counter* $+ 1$ (***A2***)
6:	***Until*** *termination condition is met* (***A3***)
7:	***Return*** $\hat{z}_{a,\varrho}^t$ (***A4***)

In Step A0, the initial CAV-dedicated lane deployment plan ($\hat{z}_{a,\varrho}^t$), set Q, passed iterations (counter) are defined. In this regard, no CAV-dedicated lanes are considered for the initial plan ($\hat{z}_{a,\varrho}^t = 0$). As no cuts are generated in the beginning, Q is an empty set ($Q = \{\}$). Also, the number of passed iterations is set to zero. In the next step, an iterative process begins. WPS is solved based on the initial CAV-dedicated lane plan ($\hat{z}_{a,\varrho}^t$) (steps W0-W7). Then, the derived worst-case potential CAV ($\hat{p}_w^{t,k}$) market size is added to set Q, as a new cut (step A1). Next, MPEC2 is solved to derive an optimal CAV-dedicated lane plan based on the updated set Q (M0-M7). Then, the number of passed iterations is updated (A2) and next, the termination condition is checked (A3). If the termination condition is not met, the preceding steps must be repeated. If the termination condition is met, the solution procedure is terminated, and the optimal CAV-dedicated lane deployment plan is returned (A4). As the termination condition, this iterative procedure continues until the WSP does not result in a worst-case total emissions cost or the algorithm reaches the determined maximum number of iterations.

MPEC2 and WPS can be classified as a mathematical program with complementarity constraints (MPCC). There exist some algorithms to solve MPCC2 and WPS, such as non-smooth penalization (Scholtes and Stöhr, 1999) and smooth regularization (Birbil et al., 2004). In this study, we adopt the Active-set algorithm, which is shown by Zhang et al. (2009) to be able to derive a strong stationary solution. It is used in several studies, mainly dealing with network design problems (Chen et al., 2016; Liu et al., 2020; Miralinaghi and Peeta, 2019; Song et al., 2017).

Fig. 4 summarizes the solution algorithm used in this study. First, the solution procedure for WSP is described. Steps W0 to W6 are applied to solve WSP. Before initiating the solution algorithms, sets Θ_0 and Θ_1 are defined in a way that $\Theta_0 = \{(w,k,t)|\hat{p}_w^{t,k} = 0\}$ and $\Theta_1 = \{(w,k,t)|\hat{p}_w^{t,k} = 1\}$ where $\Theta_0 \cup \Theta_1 = \{(w,k,t)|\forall w \in W, \forall k \in K, \forall t \in T\}and\Theta_0 \cap \Theta_1 = \varnothing$. By solving WSP, we are looking to

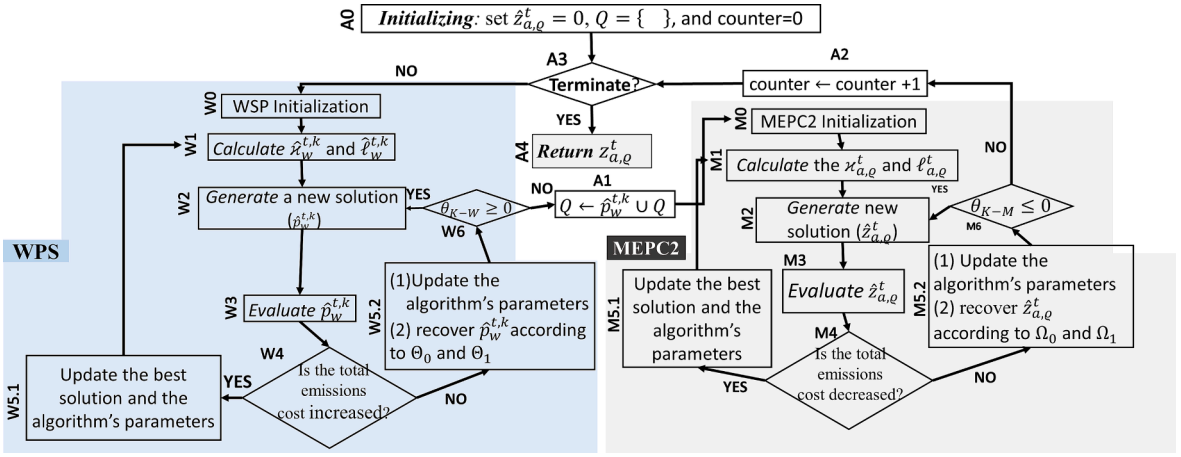

Fig. 4. Solution algorithm.

identify potential CAV market sizes that increase the total emissions cost (in contrast to MEPC2 which tries to decrease the total emissions cost). The procedure starts with initializing $\widehat{p}_w^{t,k} = 0, \Theta_0 = \{(w,k,t)|\widehat{p}_w^{t,k} = 0\}, \Theta_1 = \{(w,k,t)|\widehat{p}_w^{t,k} = 1\}, stop = 0, \text{and} \theta_{K-W} = \infty$, in step W0. In step W1, Lagrangian multipliers corresponding to $\widehat{p}_w^{t,k}$ in sets Θ_0 and Θ_1, $\widehat{x}_w^{t,k}$ and $\widehat{\prime}_w^{t,k}$, are determined. Given Lagrangian multipliers, Adjustment problem WPS (AP-W, see Appendix 1) is solved to adjust the current solution. According to the solution of AP-W, a new feasible solution is generated (W2). Then the new solution is evaluated in step W3. If the adjusted (updated) solution results in a higher total emissions cost in the network (W4), it means that an improved solution is found and sets Θ_0 and Θ_1 are updated accordingly (W5.1). Also, control parameters *stop* gets value of 0, which means that a better solution is found. The algorithm then goes to W1 to further improve the solution. However, If the feasible solution is not an improved one, $\widehat{p}_w^{t,k}$ is recovered to the previous solution and $\theta_{\text{AP}-\text{W}}$ is updated (W5.2). Updating θ_{AP-W} ensures preventing repetitive solutions that are evaluated. Then, if it is expected that the solution algorithm can provide an improved solution (W6), the algorithm goes to W2. Otherwise, the algorithm goes to A1 to update the cut set and then start finding an optimal AV-dedicated lane design solution (M0-M6).

Steps M0-M6 describe the applied Active-set solution procedure to solve the MPEC2. To solve MPEC2, the implemented algorithm starts with an initial feasible solution ($\widehat{z}_{a,\varrho}^t$) which can be described with sets $\Omega_0 = \left\{(a,\varrho,t)|\widehat{z}_{a,\varrho}^t = 0\right\}$ and $\Omega_1 = \left\{(a,\varrho,t)|\widehat{z}_{a,\varrho}^t = 1\right\}$, where $\Omega_0 \cup \Omega_1 = \{(a,\varrho,t)|\forall a \in A, 0 \le \varrho \le \Phi_a^t, \forall t \in T\}$ and $\Omega_0 \cap \Omega_0 = \varnothing$ (M0). In the next steps, the current solution is adjusted using its Lagrangian multipliers. In step M1, the Lagrangian multipliers, $\varkappa_{a,\varrho}^t$ and $\prime_{a,\varrho}^t$, associated with decision variables in Ω_0 and Ω_1, respectively, are determined. They approximate the improvement in the objective function of MPEC2 by changing the components of the current solution. To find a new feasible solution, Adjustment problem-MEPC2 (AP-M, see Appendix 1) is solved in the next step. Based on the results of AP-M, a candidate solution that is anticipated to provide the most improvement to the current total emissions cost is determined (M2). To ensure that the candidate solution improves the current total emissions cost, it is evaluated in the next steps (M3). If the new feasible solution results in an improvement (that is, a decrease) in the total emissions cost relative to the incumbent solution (M4), it is considered as the new best solution; then the sets Ω_0 and Ω_1 are updated, accordingly (M5.1). Then, the algorithm continues to step M1 to find an improved solution. However, if the feasible solution does not decrease the total emissions cost, then the incumbent feasible solution remains as is, and θ_{AP-M} is updated (M5.2). Hence, updating θ_{AP-M} may prevent obtaining the feasible solution that is just evaluated and does not result in improvement. In this case, if it is possible to find another solution (M6), the algorithm goes to M2; otherwise, it goes to A2. In the next step (A3), the termination of algorithm is checked; if the total number of iterations is higher than the maximum iteration threshold or no solution is found for WSP (stop = 1), the algorithm is terminated, and the solution is returned (A4). Otherwise, the algorithm keeps on and repeats the described procedure again.

As discussed by Lou et al. (2009), the uncertainty set contains a finite number of components, and therefore, the cutting-plane scheme terminates after a finite number of iterations. The result is a global optimal solution for MPEC1 if, in each iteration, the

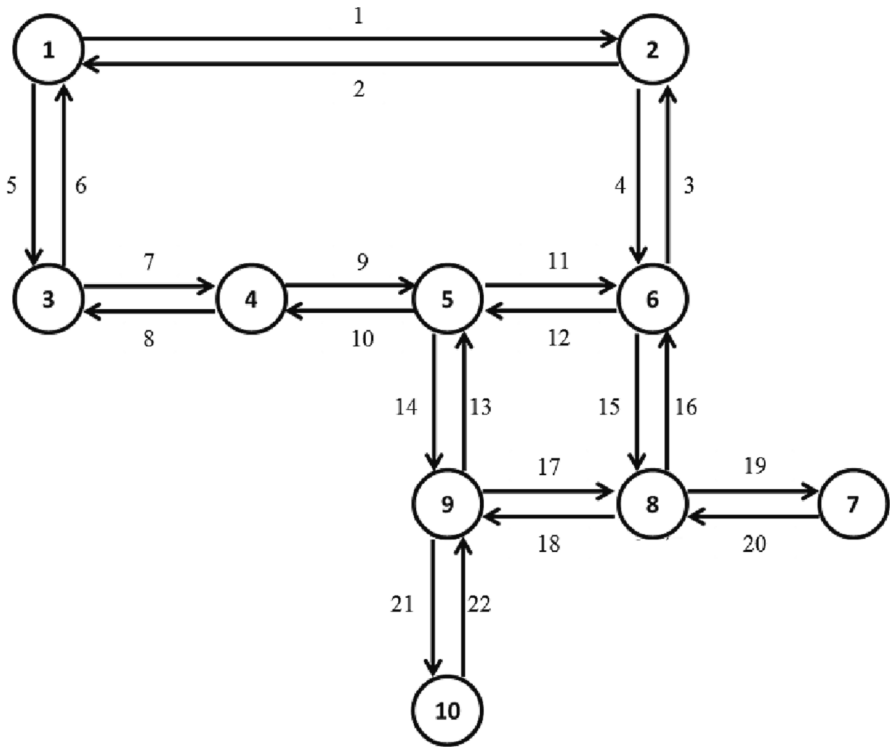

Fig. 5. Study network.

solutions are global optimum for MPEC2, and WPS. However, this is not possible since these two models are nonconvex and violate the Mangasarian-Fromovitz constraint qualification (MFCQ) at different points of feasible space. Note that a deterministic plan is solving only the MCEP2 considering set $Q = \{q|\widehat{p}_w^{t,k} = 0\}$.

6. Numerical experiment

6.1. Case study characteristics

The proposed MPEC2 problem is applied to a synthetic network (Fig. 5). The synthetic network consists of 10 nodes, 22 links, and 90O-D pairs. The planning horizon is assumed to be equal to 16 years, which is divided into four 4-years periods. During successive periods, travel demand grows at a constant rate of 5% (per planning period) across all O-D pairs. Moreover, the presented O-D travel demand in Table 3 is used for the first period without considering demand growth. However, the O-D travel demands in the following periods are derived by multiplying the corresponding growth factors by those of the first planning period. Also, the O-D pair's travel demand is assumed to be constant within each planning period. The link characteristics, including free-flow travel time and link capacity, are shown in Table 4.

As stated earlier, when CAVs move exclusively in CAV-dedicated lanes, the capacities of CAV-dedicated lanes are higher compared to GP lanes. In this study, it is assumed that the per-lane capacity triples after converting to a CAV-dedicated lane (Chen et al., 2016). According to Correia et al. (2019) and Pudāne and Correia (2020), the value of time of CAV travelers, compared to HDV travelers, could be almost 26% lower, although more research is needed on that topic. Therefore, the values of time of HDV and CAV travelers are assumed to be equal to 20 ($/h) and 15 ($/h), respectively. The rest of the numerical settings used in this research are as follows: (1) number of trips of each traveler per year: $\chi_w^t = 720$ (trip/year); (2) excess cost of using CAV:$\xi_w^t = 1000$ ($/year); (3) benefit threshold: $\overline{\mu}_w^t = 1000$ $; (4) $\varphi = 1.2$ (1/period); monetized cost of CO emission: $\vartheta = 50$ ($/ton) (Labi, 2014); (5) $\iota = 0.00005$. χ_w^t, ξ_w^t, $\overline{\mu}_w^t$, φ, and ι are selected according to Chen et al (2016) after adjusting for four-year planning periods; and (6) the share of E-HDVs (ψ^t) are 5%, 10%, 20%, and 45% over the planning horizon.

The proposed algorithms, Algorithm1 to Algorithm3, are solved by the General Algebraic Modeling System (GAMS), using CPLEX, CONOPT, and CONOPT4 solvers. The results are obtained using a Core i7 processor with a 3.2 GHz CPU and 32 GB RAM. The computation time for solving only MEPC2, to determine a deterministic plan, is about 8 min. To determine a robust plan, solving Algorithm 1 takes about 04:10 (hour:minute) while solving algorithms 2 and 3 take 04:05 and 00:05, respectively. The overall computation time is almost about solving the Algorithm 2. This is because of the cuts introduced to MEPC2, which make it more complex to solve.

7. Results and discussion

7.1. Analysis of lane reallocation policy impacts

In this section, we investigate the impacts of different lane reallocation strategies on total emissions cost, system benefit in terms of reduced emissions, and CAV market penetration rates without considering the potential CAV market size uncertainty. Under this analysis, we consider the deterministic plan based on the nominal travel demand. The existing lane widths are assumed to be equal to 12 ft, which is referred to as base case in this subsection. The total emissions cost corresponding to the deterministic plan, under the base case (12 ft), is equal to 18.49 million dollars. We consider three possible lane widths for CAV-dedicated lanes: 8 ft, 9 ft, and 10 ft. For example, metropolitan authorities can allocate 3 dedicated lanes with 8 ft width to CAVs for any two conventional 12 ft lanes. The potential CAV market size for all of the O-D pairs is assumed to be equal to 75%. The CAV market size in all O-D pairs is assumed to be equal to 10% at the beginning of the planning horizon. It should be noted that although our analysis indicates that the zero-lateral wander of CAVs can contribute to vehicle emissions reduction by reducing lane widths, there is a need to regulate the minimum lane width based on the CAV width with unfolded mirrors and CAV travelers' safety perception.

Table 3
O-D Pair Travel Demand ($\times 10^3$).

		Destination									
		1	2	3	4	5	6	7	8	9	10
Origin	1	0	0.4	0.4	2	0.8	1.2	2	3.2	2	5.2
	2	0.4	0	0.4	0.8	0.4	1.6	0.8	1.6	0.8	2.4
	3	0.4	0.4	0	0.8	0.4	1.2	0.4	0.8	0.4	1.2
	4	2	0.8	0.8	0	2	1.6	1.6	2.8	2.8	4.8
	5	0.8	0.4	0.4	2	0	0.8	0.8	2	3.2	4
	6	1.2	1.6	1.2	1.6	0.8	0	1.6	3.2	1.6	3.2
	7	2	0.8	0.4	1.6	0.8	1.6	0	4	2.4	7.6
	8	3.2	1.6	0.8	2.8	2	3.2	4	0	3.2	6.4
	9	2	0.8	0.4	2.8	3.2	1.6	2.4	3.2	0	4
	10	5.2	2.4	1.2	4.8	4	3.2	7.6	6.4	4	0

Table 4
Link Characteristics of Synthetic Network.

Link ID	From	To	Free flow Travel time (min)	Capacity $\times 10^3$ (veh/h)
1	1	2	6	26
2	2	1	6	26
3	6	2	5	14
4	2	6	5	14
5	1	3	4	24
6	3	1	4	24
7	3	4	4	18
8	4	3	4	18
9	4	5	2	18
10	5	4	2	18
11	5	6	4	14
12	6	5	4	14
13	9	5	5	10
14	5	9	5	10
15	6	8	2	14
16	8	6	2	14
17	9	8	10	16
18	8	9	10	16
19	8	7	3	18
20	7	8	3	18
21	9	10	3	8
22	10	9	3	8

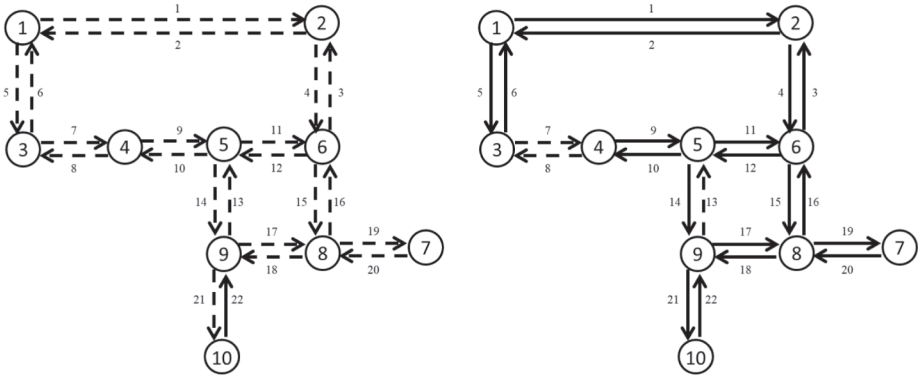

(a) 8-ft Lane reallocation policy (b) 9-ft Lane reallocation policy

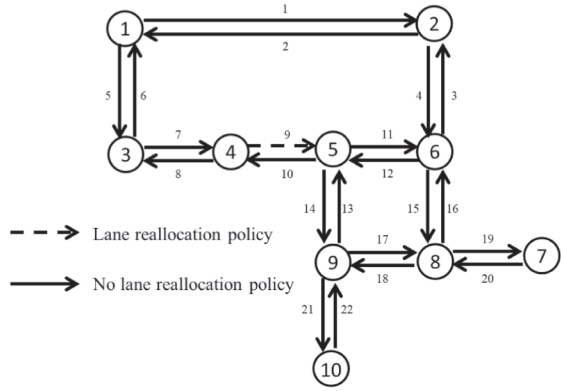

(c) 10-ft Lane reallocation policy

Fig. 6. CAV-dedicated lane deployment plan.

First, we illustrate different lane reallocation strategies, in terms of lane width in the last period in Fig. 6. In this figure, the CAV-dedicated links that are deployed under lane reallocation policy, are shown in dash arrows. Due to the convenience of applying the 8-ft lane reallocation policy (as for every two 12-ft lanes, there are three 8-ft CAV-dedicated lanes), the 8-ft lane reallocation policy is applied more than others during the planning horizon. On the other hand, the 10-ft lane reallocation policy is applied only once. Table 5 summarizes the total emissions costs of different CAV-dedicated lane deployment plans and a do-nothing plan. The do-nothing plan refers to the plan under which there are no CAV-dedicated lanes. Regardless of how the lane reallocation policy is implemented, CAV-dedicated lane deployment plans reduce total system emissions costs by more than 14% compared to the do-nothing plan without CAV-dedicated lanes.

Next, the total system benefits under different lane reallocation policies are shown in Fig. 7. The total system benefit is equal to the difference in total emissions costs after employing the lane reallocation strategy relative to the base case (12 ft). This diagram shows how increasing the road capacity as a result of reduced CAV-dedicated lane width can improve system performance by increasing total system benefits and decreasing total emissions cost. More specifically, considering the 10-ft, 9-ft, and 8-ft CAV-dedicated lanes result in 4.57%, 3.72%, and 2.26% improvement in total emissions cost relative to the 12-ft lane case, respectively. Moreover, the improvements account for 0.85, 0.69, and 0.42 million dollars of total system benefits relative to the 12-ft lane case, with respect to 10-ft, 9-ft, and 8-ft CAV-dedicated lanes.

7.2. Analysis of robust design impacts on vehicle emissions

To understand the importance of considering CAV demand uncertainty, the CAV-dedicated lane deployment is investigated under deterministic and robust plans. Under the deterministic plan, the potential CAVMPs are equal to the nominal values (75% during the planning horizon). The robust plans consider the possible deviation of the deterministic values from the nominal values. For each period, we assume five sets of uncertainty for the potential CAV market size of each O-D pair. The potential CAV market sizes of uncertainty sets are:

(1) Set 1: 75% (nominal value)
(2) Set 2: 70%
(3) Set 3: 80%
(4) Set 4: 65%
(5) Set 5: 60%

Four different robust plans are considered based on the lane reallocation policies, including (i) Robust (12 ft), (ii) Robust_LRP10 (10 ft), (iii) Robust_LRP9 (9 ft), and (iv) Robust_LRP8 (8 ft). The uncertainty budget is set at 27O-D pairs under all robust plans. To evaluate the performance of the deterministic and robust plans, we carried out the Monte Carlo simulation technique for different CAV-dedicated lane deployment plans. The performance of the defined plans is compared across five realized travel demand cases, ranging from pessimistic (Case 1) to optimistic (Case 5). Each simulation case has a specific share of Set 1, Sets 2 and 3, and Sets 4 and 5, as stated earlier. These shares are chosen randomly based on a uniform distribution. For example, in Case 2, 18 O-D pairs have deterministic CAVMPs (Set 1) and 63O-D pairs belong to Set 4 or Set 5. Overall, Case 1 is considered the most pessimistic case, given the high shares of Sets 4 and 5. On the other hand, Case 5 is assumed to be the most optimistic case due to the high share of Set 1 and the low share of Sets 4 and 5. The other simulation cases (Cases 2 to 4) have some optimism due to the increase in the shares of Sets 1, 2, and 3, and some pessimism due to the decrease in the shares of Sets 4 and 5. The descriptions of simulation cases are summarized in Table 6.

Table 7 shows the average, maximum, minimum, and standard deviations of the total emissions costs of deterministic and robust CAV-dedicated lane plans under the five simulation cases. Overall, the robust plans have superior performance in terms of average, max, min, and standard deviation of total emissions cost compared to the deterministic plan under the pessimistic cases (Cases 1–3). On the other hand, the deterministic plan outperforms the robust plan under optimistic cases (Cases 4–5) since the robust plan accounts for the worst-case demand scenario while the deterministic plan factors in the nominal values of CAVMP. Moreover, the robust plan shows better performance in all five cases in terms of standard deviation. This is because multiple sets of potential CAV market sizes are captured in the design to determine a robust optimal plan.

Next, the benefits of lane reallocation policies in robust planning are discussed. The results shown in Table 7 demonstrate the improvements in robust planning after the lane reallocation policies are implemented. When lane reallocation policy is used in robust planning, robust plans (Robust-LRP8, Robust-LRP9, and Robust-LRP10) outperform deterministic plans in all simulation cases

Table 5
Total emissions cost of CAV-dedicated lane deployment plans.

CAV-dedicated lane deployment		Total emissions cost (Million $)	Improvement in total emissions cost relative to do-nothing plan (%)
Lane width	8 (ft)	17.65	18.55%
	9 (ft)	17.81	17.83%
	10 (ft)	18.08	16.58%
	12 (ft)	18.49	14.65%
Do-nothing plan		21.67	–

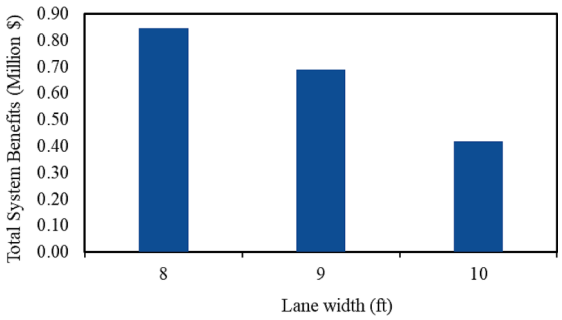

Fig. 7. Impacts of lane reallocation policy on total system benefit in terms of emissions cost.

Table 6
Description of simulation cases.

		Number of O-D pairs		
	Simulation	Set 1 (Deterministic)	Set 2 and 3	Set 4 and 5
Pessimistic	Case 1	0	0	90
	Case 2	18	9	63
	Case 3	36	18	36
	Case 4	54	27	9
Optimistic	Case 5	81	9	0

Table 7
Comparison of robust and deterministic plans using simulation.

	Simulation case	Measurement	Deterministic	Robust	Robust-LRP10	Robust-LRP9	Robust-LRP8
Pessimistic	Case 1	Average (Million $)	20.58	19.49	19.18	19.05	18.94
		Maximum (Million $)	20.93	19.59	19.28	19.15	19.04
		Minimum (Million $)	20.27	19.37	19.07	18.93	18.81
		Standard Deviation (Thousand $)	152.48	51.10	49.58	48.88	51.00
	Case 2	Average (Million $)	20.19	19.18	18.91	18.79	18.70
		Maximum (Million $)	21.65	20.12	19.92	19.84	19.76
		Minimum (Million $)	19.51	18.84	18.54	18.41	18.33
		Standard Deviation (Thousand $)	459.69	162.26	173.03	180.57	186.57
	Case 3	Average (Million $)	19.38	18.79	18.53	18.42	18.32
		Maximum (Million $)	20.54	19.28	19.10	19.03	18.96
		Minimum (Million $)	18.85	18.43	18.19	18.09	18.00
		Standard Deviation (Thousand $)	317.23	151.45	160.51	165.25	170.94
	Case 4	Average (Million $)	18.61	18.28	18.05	17.95	17.86
		Maximum (Million $)	19.06	18.77	18.61	18.54	18.47
		Minimum (Million $)	18.28	17.96	17.75	17.66	17.57
		Standard Deviation (Thousand $)	137.61	120.09	118.38	118.49	118.89
Optimistic	Case 5	Average (Million $)	18.37	18.09	17.88	17.78	17.70
		Maximum (Million $)	18.47	18.18	17.98	17.88	17.80
		Minimum (Million $)	18.29	18.00	17.79	17.70	17.61
		Standard Deviation (Thousand $)	32.80	32.13	31.80	31.75	31.63

(regardless of measurement). These improvements imply that a lane reallocation policy can also address the demand uncertainty. Applying lane reallocation policy, in particular, improves the performance of robust plans in terms of average, maximum, and minimum total system emissions cost. Also, smaller lane width results in more improvements. For instance, Robust_LRP8, Robust_LRP9, and Robust_LRP10 have the best performance, in that order. The comparative pattern of standard deviation between robust plans is different. Overall, employing lane reallocation policies in robust planning increases the standard deviations of the total emissions costs, and this increment is greater in lane reallocation policies with lower lane width. The discussed pattern of standard deviation among robust plans cannot be viewed as a disadvantage of lane reallocation policies, as lane reallocation policies have already demonstrated their superiority in terms of maximum and minimum total emissions cost. In other words, although lane reallocation policies (and among them, lower lane widths) have higher standard deviations, these deviations are located in lower ranges of total emissions costs, based on the lower maximum and minimum total emissions cost.

The effects of potential CAV market size are also highlighted in Table 7. The performance of the optimal plans (deterministic and robust plans) improved from Case 1 to Case 5. This implies that the impact of uncertainty of consumers' willingness to purchase CAVs on vehicle emissions can be reduced by motivating travelers to purchase CAVs.

Next, another type of simulation is carried out to provide more insights into the deterministic and robust plan's performance. In these simulations, uncertain sets are assumed to have different shares of 9, 18, 27, 36, 45, 54, 63, 72, 81, and 90O-D pairs in each planning horizon. For simplicity, the share of Set 2 is considered 0, over all of the simulations. Next, every possible combination of potential CAV market penetration size sets is detected, and O-D pairs are assigned randomly to the uncertain sets in such a way that the number of assigned O-D pairs to each uncertain set is equal to the share of uncertain sets. As an example, consider the following combinations of uncertain sets: Set 1 (18O-D pairs), Set 2 (0 O-D pairs), Set 3 (9 O-D pairs), Set 4 (45O-D pairs), and Set 5 (18O-D pairs). After randomly assigning O-D pairs to uncertain sets, O-D pairs (1,5), (2,7), (6,9), (10,3), (4,8), (7,3), (2,5), (4,7), (3,10) are assigned to Set 4 and their corresponding potential CAV market size will be 60%. Finally, the optimal CAV-dedicated plan is evaluated regarding the determined uncertain sets. As this assignment procedure is random (with uniform distribution), it repeats several times for each combination. Then, the average of the generated total emissions costs is derived as an indicator for the performance of the optimal CAV-dedicated plan under each combination.

Fig. 8 shows the estimated density distribution (more specifically, the kernel density estimation) of the observed total emissions cost of deterministic and robust plans for the simulations described. The deterministic plan shows a wider range of observed total emissions costs and a lower mode, but higher average value, under the simulation cases compared to the robust plans. This implies higher variation and standard deviation compared to the robust plans, which is consistent with the results of Table 7. This is due to the fact that the deterministic plan concentrates on only one uncertainty set (Set 1, which has the deterministic values). On the other hand, to determine robust plans, several sets of possible potential CAV market sizes (due to the cutting-plane algorithm application) are considered. As a result, robust plans lower the total emissions costs of a wider range of potential CAV market sizes. Also, the benefits of the lane reallocation policy are highlighted. The lane reallocation policy reduces the maximum and minimum of the simulated total emissions cost range compared to those under the robust plans. Moreover, the modes of the total emissions cost are smaller due to the lane reallocation policies. It means that under lane reallocation policy the total emissions costs tend to be on the lower side. In particular, lane reallocation policies with smaller lane widths are more effective in this regard due to the fact that they use the available road space more efficiently and thus provide more capacity for CAVs. The discussed benefits of lane reallocation policies are consistent with the discussed results in Table 7.

Furthermore, based on the numerical results of these simulations, the effects of CAV promotion on the performances of the deterministic plan and the robust plan are investigated. To do this, the performance of the optimal plans under different shares of uncertainty sets are discussed. In the first set of analyses, the density distribution of average emissions costs for the deterministic and robust plans are discussed. Fig. 9 shows the density distribution of the deterministic plan and robust plan under three levels of uncertainty set 3 (which has a CAV potential size of 80%) and three levels of uncertainty set 5 (which has a 60% CAV potential size). Each demonstrated density distribution, for example the density distribution with a 30% share of set 3 for the deterministic plan in Fig. 9(a), shows an estimated density distribution (more specifically, kernel density estimation) of the average emissions costs of the simulation cases that have a 30% share of uncertainty set 3. According to Fig. 9(a), an increase in the share of uncertainty set 3 (which has a CAV potential size of 80%) yields lower average emissions costs, for both the deterministic and robust plans. On the other hand, increasing the share of uncertainty set 5 (which has a 60% CAV potential size) has negative impacts on the performance of the optimal plans and increases their corresponding emissions costs (Fig. 9(b)). This highlights the fact that increasing the CAV potential size, or, in other words, promoting CAVs, results in better performance in terms of the emissions cost of the system.

In the next set of analysis, the interactions of three uncertainty sets, sets 3–5, are considered to investigate the effects of CAV promotions on the performance of deterministic and robust plans (Fig. 10). As stated before, under these simulations, uncertainty sets can have shares of 9, 18, …, and 90O-D pairs. To have continuous plots in Fig. 10, the points between these values are interpolated. Each of the shown plots represents the average emissions costs corresponding to different shares of uncertainty sets 3–5 under the deterministic or robust plans. Average emissions costs are shown in in a range of colors. The blue area denotes the lower average emissions costs while the red area indicates the higher average emissions costs. Similar to the observations and discussions of Fig. 9,

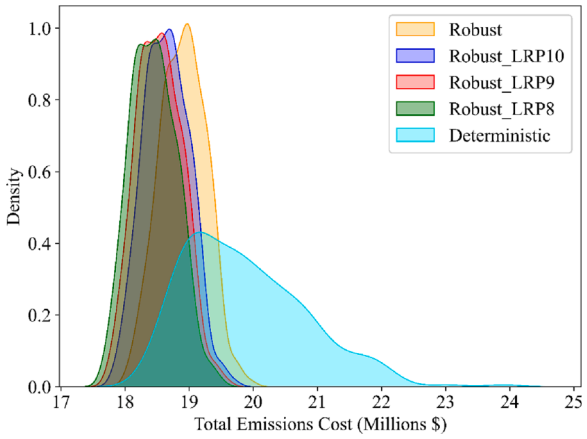

Fig. 8. Distribution of simulated total emissions costs under deterministic and robust plans.

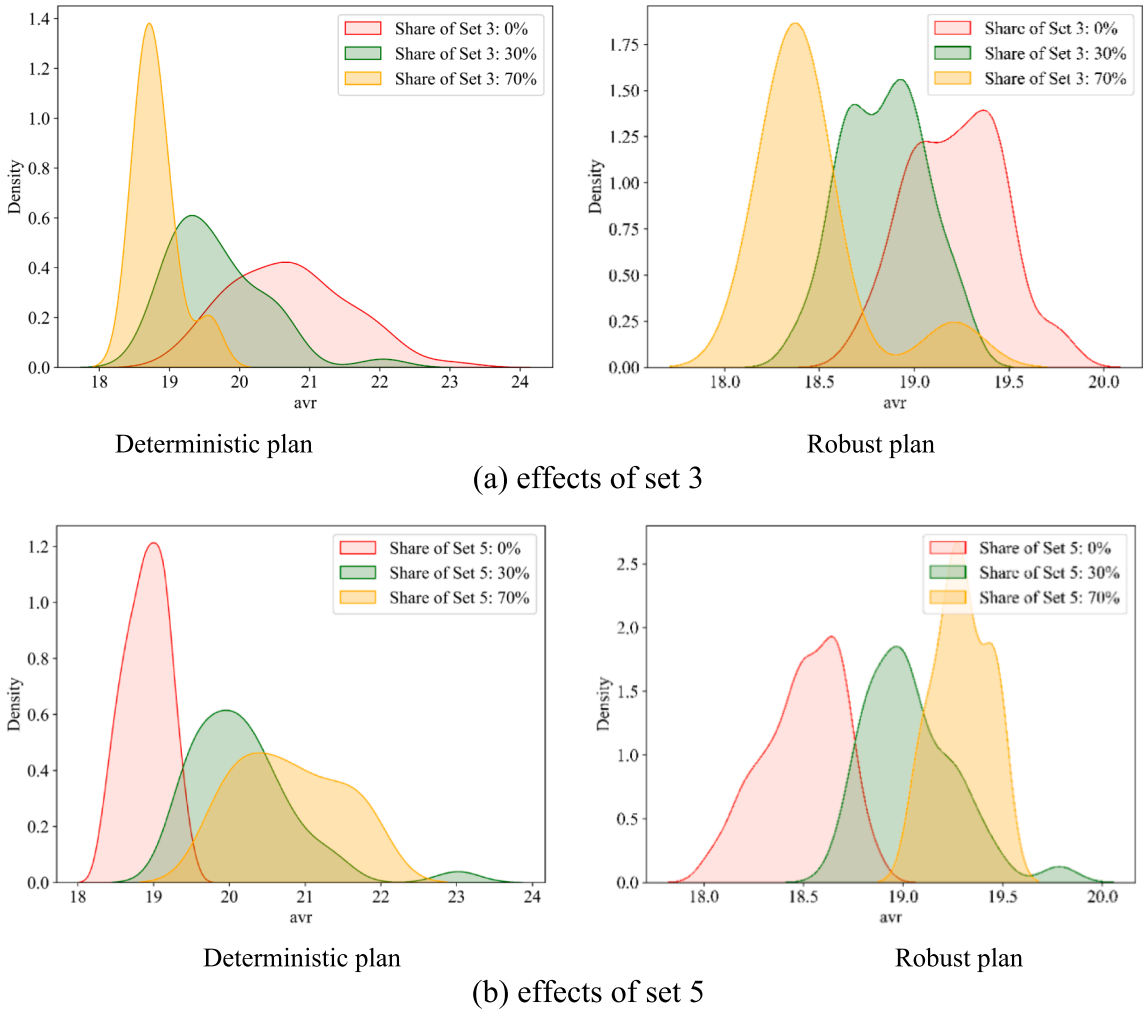

Fig. 9. Effects of CAV promotion on density distribution of emissions costs under deterministic and robust plans.

levels of CAV potential sizes have important effects on the performance of optimal plans. More specifically, considering each of the shown plots in Fig. 10, decreasing the share of uncertainty sets 4 and 5 (which their CAV potential sizes are lower than the nominal value) contributes to emissions costs improvements, under both deterministic and robust plans. On the other hand, increasing the share of set 3 (which has a higher CAV potential size relative to the nominal value) improves the performance of the optimal plans by reducing the emissions costs. This is because the high share of set 3 leads to a higher CAV adoption rate, which improves traffic flow mobility. This implies that if metropolitan authorities motivate travelers to purchase CAVs, then the higher CAV adoption rate reduces the impact of forecast uncertainty of the potential CAV market size on total emissions cost.

8. Concluding remarks

This study proposed a robust optimization model to deploy CAV-dedicated lanes in a highway network to address the inherent uncertainty in the forecast of the potential CAV market size. This model is formulated as a bi-level framework. The upper-level model captures the goal of metropolitan authorities, which in this study is to minimize the worst-case vehicle emissions under different possible realized potential CAV market sizes by identifying the optimal links and number of allocated lanes. Given CAVs' relatively small lateral wander and, consequently, their requirement for smaller lane widths, it is possible, for wide roadways, to reallocate lanes for shared use of the road corridor by HDVs and CAVs. In such lane reallocation, the total number of lanes can be increased. The lower-level model captures the route and vehicle type choices of travelers using the equilibrium condition and demand diffusion models, respectively. The bi-level model is formulated as a min–max mathematical program with equilibrium conditions and solved using the cutting-plane scheme and active-set algorithm.

Our computational experiments demonstrate that long-term scheduling of CAV-dedicated lanes via lane reallocation is feasible and that it can lead to a significant reduction in total emissions costs. Specifically, it can provide a significant reduction in vehicle emissions

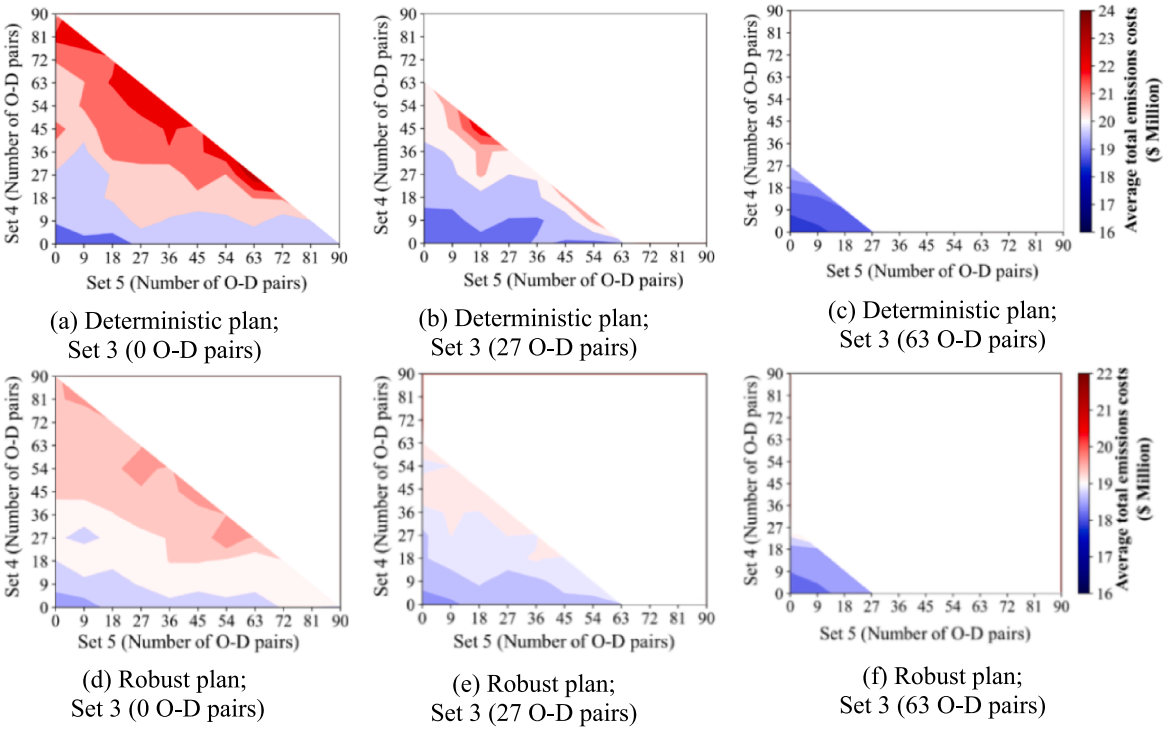

Fig. 10. Effects of uncertainty sets interactions on emissions costs.

costs. Besides the benefits of reduced total emissions costs, lane reallocation policy contributes to the promotion of CAVs in the network. After evaluation of deterministic and robust plans using the Monte Carlo simulation technique, the deterministic plan shows a wider range of total emissions costs in the corresponding distribution. On the other hand, robust plans concentrate on limited ranges of total emissions costs. This implies a reduction in the uncertainty of potential total emissions costs in the future. Furthermore, lane reallocation policy improves robust design by lowering the average, maximum, minimum, and standard deviation of total emissions costs. Thus, it can be considered a synergistic policy for addressing potential CAV market size uncertainty. Also, our computational experiments indicate that the impact of the uncertainty of consumers' willingness to purchase CAVs on vehicle emissions can be reduced by motivating travelers to purchase CAVs. It is worth noting, however, that there will be other factors that will influence consumers' willingness to purchase CAVs, and some of these factors may include the quality and quantity of supporting infrastructure and the availability of skilled repair technicians.

This research can be extended in several directions. First, this research assumes uncertainty only in the forecast of potential CAV market size over the planning horizon. However, given the long-term nature of the planning horizon, there is uncertainty in the forecast of aggregate travel demand for CAVs and HDVs. This is due to changes in economic and demographic conditions. There is a need for a future study that develops a robust optimization model that accounts for the uncertainty in aggregate travel demand. Second, the present study assumes that travelers have an identical value of time in their route choice. However, in practice, travelers have different values of time (Miralinaghi et al., 2019; Seilabi et al., 2020). In addition, HDVs and CAVs have different values of time (Seilabi et al., 2022). Therefore, it is necessary to formulate the lower-level model as multi-class equilibrium conditions that capture the different values of time among travelers. Third, this study assumes that all CAVs are EVs, while currently there are CAVs that are manufactured as ICEVs. Although this is consistent with several automakers' plans to use electricity as the power source for future autonomous vehicles (General Motors, 2022; Gurman, 2021; Tesla, 2021; Valdes-Dapena, 2018), it is interesting to include this category of CAVs in the analysis as well.

CRediT authorship contribution statement

Sania E. Seilabi: Conceptualization, Formal analysis, Investigation, Methodology, Resources, Validation, Visualization, Writing – original draft, Writing – review & editing. **Mohammadhosein Pourgholamali:** Formal analysis, Investigation, Methodology, Resources, Software, Validation, Visualization, Writing – original draft, Writing – review & editing. **Gonçalo Homem de Almeida Correia:** Methodology, Supervision, Writing – review & editing. **Samuel Labi:** Supervision, Methodology, Writing – review & editing, Funding acquisition.

Declaration of Competing Interest

The authors declare that they have no known competing financial interests or personal relationships that could have appeared to influence the work reported in this paper.

Acknowledgments

This study is based on research supported by the Center for Connected and Automated Transportation (CCAT), Region V University Transportation Center funded by the U.S. Department of Transportation, Award #69A3551747105. Any errors are those of the authors alone.

Author Contributions

The authors confirm contribution to the paper as follows: all authors contributed to all sections. All authors reviewed the results and approved the final version of the manuscript.

Appendix

In this section, the sub-problems used in main model reformulation or solution algorithms are presented. First, MPEC1 is reformulated as a mathematical program with equilibrium constraints (MPEC2) as follows:

$$\min_{z,v,p} \omega \tag{27}$$

$$\sum_{t}\sum_{a} \kappa e_a^t\left(\nu_a^{t,q}\right)\nu_a^{t,q} \le \omega \,\forall q \in Q \tag{28}$$

$$\nu_a^{t,q} \in V(q) \forall q \in Q \,\forall a \in A, \forall t \in T \tag{29}$$

$$\tau_a^{t,q}\left(\nu_a^{t,q},\, c_a^t\right) = \tau_a^0 \bullet \left(1 + 0.15\left(\frac{\nu_a^{t,q}}{\zeta_{\overline{a}}^t}\right)^4\right) \forall q \in Q,\ \forall a \in A, \forall t \in T \tag{30}$$

$$0 \le x_{a,w}^{n,t,q} \perp \left(\tau_a^{t,q}\left(\nu_a^{t,q}, \zeta_{\overline{a}}^t\right) + \pi_{i,w}^{n,t,q} - \pi_{j,w}^{n,t,q}\right) \ge 0 \forall n \in N, \forall w \in W, \forall t \in T\, \forall (i,j) = a \in A \backslash \overline{A},\ \forall q \in Q \tag{31}$$

$$0 \le x_{\overline{a},w}^{n,t,q} \perp \left(\tau_{\overline{a}}^{t,q}\left(\nu_{\overline{a}}^{t,q}, \zeta_{\overline{a}}^t\right) + \pi_{i,w}^{n,t,q} - \pi_{j,w}^{n,t,q} - \theta_{\overline{a}}^{n,t,q}\right) \ge 0\, \forall n \in N, \forall w \in W, \forall t \in T,\ \forall (i,j) = \overline{a} \in \overline{A},\ \forall q \in Q \tag{32}$$

$$x_{\overline{a},w}^{n,t,q} = 0 \,\forall n \in \{1,2\},\ \forall w \in W, \forall t \in T, \forall \overline{a} \in \overline{A},\ \forall q \in Q \tag{33}$$

$$x_{\overline{a},w}^{2,t,q} \le M \bullet \sum_{i=1}^{t}\sum_{\varrho=1}^{\Phi_a^t} z y_{\overline{a},\varrho}^{i} \,\forall w \in W, \forall t \in T, \forall \overline{a} \in \overline{A},\ \forall q \in Q \tag{34}$$

$$x_{\overline{a},w}^{n,t,q} \bullet \theta_{\overline{a}}^{n,t,q} = 0 \,\forall n \in N, \forall w \in W, \forall t \in T,\ \forall \overline{a} \in \overline{A},\ \forall q \in Q \tag{35}$$

$$\theta_{\overline{a}}^{n,t,q} \ge 0 \,\forall n \in N, \forall t \in T, \forall \overline{a} \in \overline{A},\ \forall q \in Q \tag{36}$$

$$\zeta_{\overline{a}}^t = \zeta_{\overline{a}}^{t-1} + \phi_{\overline{a}} \sum_{\varrho=1}^{\Phi_a^t} 2^{\varrho-1} \times z_{a,\varrho}^t \,\forall \overline{a} \in \overline{A},\ \forall t > 1 \tag{37}$$

$$\zeta_{\overline{\overline{a}}}^t = \zeta_{\overline{\overline{a}}}^{t-1} - \phi_{\overline{\overline{a}}} \sum_{\varrho=1}^{\Phi_a^t} 2^{\varrho-1} \times z_{a,\varrho}^t \,\forall \overline{\overline{a}} \in \overline{\overline{A}}, \forall t > 1 \tag{38}$$

$$u_{\overline{a}} \bullet \left(\sum_{i=1}^{t}\sum_{\varrho=1}^{\Phi_a^t} 2^{\varrho-1} \times z_{a,\varrho}^t\right) \le u_{\overline{\overline{a}}} \bullet \left(\sum_{i=1}^{t}\sum_{\varrho=1}^{\Phi_a^t} 2^{\varrho-1} \times z_{a,\varrho}^t\right) \forall t \in T,\ \forall [\overline{\overline{a}}, \overline{a}] \in H \tag{39}$$

$$x_{\overline{a},w}^{2,t} \le M \bullet \sum_{i=1}^{t}\sum_{\varrho=1}^{\Phi_a^t} 2^{\varrho-1} \times z_{a,\varrho}^t \,\forall w \in W, \forall t \in T, \forall \overline{a} \in \overline{A} \tag{40}$$

(1)-(6), (11).

where the superscript $(\bullet)^q$ denotes the variables that are associated with a specific potential CAV market size scenario $q \in Q$.

Next, the second sub-problem, WPS, is presented as follows:

$$\max_{p} \sum_{t} \sum_{a} \kappa e_a^t\left(\nu_a^t, c_a^t\right).\nu_a^t \tag{41}$$

$$\tau_a^t\left(\nu_a^t, \varsigma_{\bar{a}}^t\right) = \tau_a^0 \bullet \left(1 + 0.15\left(\frac{\nu_a^t}{\varsigma_{\bar{a}}^t}\right)^4\right) \forall a \in A \tag{42}$$

$$0 \le x_{a,w}^{n,t} \perp \left(\tau_a^t\left(\nu_a^t, \varsigma_{\bar{a}}^t\right) + \pi_{i,w}^{n,t} - \pi_{j,w}^{n,t}\right) \ge 0 \,\forall n \in N, \forall w \in W, \forall t \in T, \forall (i,j) = a \in A \backslash \overline{A} \tag{43}$$

$$0 \le x_{\bar{a},w}^{n,t} \perp \left(\tau_{\bar{a}}^t\left(\nu_{\bar{a}}^t, \varsigma_{\bar{a}}^t\right) + \pi_{i,w}^{n,t} - \pi_{j,w}^{n,t} - \theta_{\bar{a}}^{n,t}\right) \ge 0 \,\forall n \in N, \forall w \in W, \forall t \in T, \forall (i,j) = \bar{a} \in \overline{A} \tag{44}$$

$$x_{\bar{a},w}^{n,t} = 0 \,\forall n \in \{1,2\},\ \forall w \in W, \forall t \in T, \forall \bar{a} \in \overline{A} \tag{45}$$

$$x_{\bar{a},w}^{2,t} \le M \bullet \sum_{i=1}^{t} \sum_{\varrho=1}^{\Phi_a^t} 2^{\varrho-1} \times \hat{z}_{a,\varrho}^t \,\forall w \in W, \forall t \in T, \forall \bar{a} \in \overline{A} \tag{46}$$

$$x_{\bar{a},w}^{n,t} \bullet \theta_{\bar{a}}^{n,t} = 0 \,\forall n \in N, \forall w \in W, \forall t \in T, \forall \bar{a} \in \overline{A} \tag{47}$$

$$\theta_{\bar{a}}^{n,t} \ge 0 \,\forall n \in N, \forall t \in T, \forall \bar{a} \in \overline{A} \tag{48}$$

(1)-(3)(6).

All of the included constraints ((1)-(6), (41)-(48)) have similar concepts to the ones in MPEC1 ((1)-(9), (11)-(26)).

In the following, the sub-problems that are used in the solution algorithm are presented. To determine a new potential solution to MEPC2, or in other word, to adjust the current solution of MEPC2, according to the Lagrangian multipliers, it is required to solve the AP-M ((49)-(53)) in step M2.

$$\min_{h,g} \sum_{(a,\varrho,t)\in\Omega_0} g_{a,\varrho}^t \varkappa_{a,\varrho}^t - \sum_{(a,\varrho,t)\in\Omega_1} h_{a,\varrho}^t \not{\varkappa}_{a,\varrho}^t \tag{49}$$

$$\begin{aligned} & u_{\bar{a}} \bullet \left(\sum_{i=1}^{t} \sum_{\varrho=1}^{\Phi_a^t} 2^{\varrho-1} \times z_{a,\varrho}^t \sum_{i=1}^{t} \sum_{\varrho=1}^{\Phi_a^t} 2^{\varrho-1} \times g_{a,\varrho}^t - \sum_{i=1}^{t} \sum_{\varrho=1}^{\Phi_a^t} 2^{\varrho-1} \times h_{a,\varrho}^t\right) \\ & \le u_{\bar{\bar{a}}} \left(\sum_{i=1}^{t} \sum_{\varrho=1}^{\Phi_a^t} 2^{\varrho-1} \times z_{a,\varrho}^t + \sum_{i=1}^{t} \sum_{\varrho=1}^{\Phi_a^t} 2^{\varrho-1} \times g_{a,\varrho}^t - \sum_{i=1}^{t} \sum_{\varrho=1}^{\Phi_a^t} 2^{\varrho-1} \times h_{a,\varrho}^t\right) \forall \bar{a}, a, \bar{\bar{a}} \in \overline{\overline{A}} \end{aligned} \tag{50}$$

$$\sum_{\varrho=1}^{\Phi_a^t} 2^{\varrho-1} \times z_{a,\varrho}^{t-1} + \sum_{\varrho=1}^{\Phi_a^t} 2^{\varrho-1} \times g_{a,\varrho}^{t-1} - \sum_{\varrho=1}^{\Phi_a^t} 2^{\varrho-1} \times h_{a,\varrho}^{t-1} \le \sum_{\varrho=1}^{\Phi_a^t} 2^{\varrho-1} \times z_{a,\varrho}^t + \sum_{\varrho=1}^{\Phi_a^t} 2^{\varrho-1} \times g_{a,\varrho}^t - \sum_{\varrho=1}^{\Phi_a^t} 2^{\varrho-1} \times h_{a,\varrho}^t \,\forall t \in T,\ \forall a \in \overline{A} \tag{51}$$

$$\sum_{(a,\varrho,t)\in\Omega_0} g_{a,\varrho}^t \varkappa_{a,\varrho}^t - \sum_{(a,\varrho,t)\in\Omega_1} h_{a,\varrho}^t \not{\varkappa}_{a,\varrho}^t > \theta_{K-M} \tag{52}$$

$$g_{a,\varrho}^t, h_{a,\varrho}^t \in \{0,1\}\ (a,\varrho,t) \in \Omega_0 \cup \Omega_1 \tag{53}$$

where equation (50) ensures that according to the new solution, the total width of CAV-dedicated lanes does not exceed the provided space by converting GP lanes, for each link. Equation (51) satisfies the deployment of CAV-dedicated lanes over the planning horizon. Equation (52) prevents getting a solution that is already found which did not improve the current optimal solution. Decision variables are binary in this problem (Equation (53)).

Adjustment problem-WPS (AP-W) ((54)-(58)) is solved to provide an improved solution to WSP (step W2), based on the Lagrangian multipliers.

$$\max_{h,g} \sum_{(w,k,t)\in\Theta_0} \hat{g}_w^{t,k} \hat{\varkappa}_w^{t,k} - \sum_{(w,k,t)\in\Theta_1} \hat{h}_w^{t,k} \not{\hat{\varkappa}}_w^{t,k} \tag{54}$$

$$\sum_{(w,k)\in\Theta_0} \hat{g}_w^{t,k} - \sum_{(w,k)\in\Theta_1} \hat{h}_w^{t,k} + \sum_{(w)} \sum_{k=2}^{|K|} p_w^{t,k} \le \Lambda^t \,\forall t \in T \tag{55}$$

$$\sum_{(k)\in\Theta_0} \hat{g}_w^{t,k} - \sum_{(k)\in\Theta_1} \hat{h}_w^{t,k} + \sum_{k=2}^{|K|} p_w^{t,k} \le 1 \,\forall t \in T,\ \forall w \in W \tag{56}$$

$$\sum_{(w,k,t)\in\Theta_0} \widehat{g}_w^{t,k}\widehat{x}_w^{t,k} - \sum_{(w,k,t)\in\Theta_1} \widehat{h}_w^{t,k}\widehat{\ell}_w^{t,k} < \theta_{K-W} \tag{57}$$

$$\widehat{g}_w^{t,k}, \widehat{h}_w^{t,k} \in \{0,1\} \forall (w,k,t) \in \Theta_0 \cup \Theta_1 \tag{58}$$

Equation (55) satisfies the uncertainty budget in each period of time. Equation (56) ensures that at most one uncertain scenario is selected for each O-D pair. Equation (57) prevents having repetitive solutions. Decision variables are binary (equation (58)).

References

Federal Highway Administration, 2022. President Biden, USDOT Announce New Guidance and $6.4 Billion to Help States Reduce Carbon Emissions Under the Bipartisan Infrastructure Law [WWW Document]. URL https://highways.dot.gov/newsroom/president-biden-usdot-announce-new-guidance-and-64-billion-help-states-reduce-carbon (accessed 3.4.23).

Ajanovic, A., Haas, R., 2016. Dissemination of electric vehicles in urban areas: Major factors for success. Energy 115, 1451–1458. https://doi.org/10.1016/j.energy.2016.05.040.

Bazaraa, M.S., Sherali, H.D., Shetty, C.M., 2013. Nonlinear Programming: Theory and Algorithms. John Wiley & Sons, Hoboken, NJ.

Bertsimas, D., Sim, M., 2003. Robust discrete optimization and network flows. Math Program 98, 49–71. https://doi.org/10.1007/s10107-003-0396-4.

Birbil, Ş.I., Fang, S.C., Han, J., 2004. An Entropic Regularization Approach for Mathematical Programs with Equilibrium Constraints. Comput Oper Res 31, 2249–2262. https://doi.org/10.1016/S0305-0548(03)00176-X.

Center, V., 2015. Laying the Groundwork for Smart Connected Cities. USDOT, Cambridge, Massachusetts.

Chang, C.M., 2019. Asset Management Systems for a Sustainable Development of Smart Cities. In: International Conference on Smart Cities. Seoul, Korea, pp. 16–20.

Chen, Z., He, F., Zhang, L., Yin, Y., 2016. Optimal Deployment of Autonomous Vehicle Lanes with Endogenous Market Penetration. Transp Res Part C Emerg Technol 72, 143–156. https://doi.org/10.1016/J.TRC.2016.09.013.

Chen, S., Wang, H., Meng, Q., 2019. Designing Autonomous Vehicle Incentive Program with Uncertain Vehicle Purchase Price. Transp Res Part C Emerg Technol 103, 226–245. https://doi.org/10.1016/j.trc.2019.04.013.

Correia, G.H.A., Looff, E., Van Cranenburgh, S., Snelder, M., Van Arem, B., 2019. On the Impact of Vehicle Automation on the Value of Travel Time While Performing Work and Leisure Activities in a Car: Theoretical Insights and Results From a Stated Preference Survey. Transp Res Part A Policy Pract 119, 359–382. https://doi.org/10.1016/j.tra.2018.11.016.

Das, K., Sharma, S., 2022. Chapter 5 - Eco-routing navigation systems in electric vehicles: A comprehensive survey. In: Krishnamurthi, R., Kumar, A., Gill, S.S. (Eds.), Autonomous and Connected Heavy Vehicle Technology, Intelligent Data-Centric Systems. Academic Press, pp. 95–122. https://doi.org/10.1016/B978-0-323-90592-3.00006-9.

Dennis, E.P., Spulber, A., Kuntzsch, R., Neuner, R., 2017. Planning for Connected and Automated Vehicles [WWW Document]. Public Sector Consultants and Center for Automotive Research. https://www.cargroup.org/wp-content/uploads/2017/03/Planning-for-Connected-and-Automated-Vehicles-Report.pdf.

Dunn, J.B., Gaines, L., Sullivan, J., Wang, M.Q., 2012. Impact of recycling on cradle-to-gate energy consumption and greenhouse gas emissions of automotive lithium-ion batteries. Environ Sci Technol 46, 12704–12710. https://doi.org/10.1021/ES302420Z/SUPPL_FILE/ES302420Z_SI_001.PDF.

Federal Highway Administration, 2018. How Does a "Smart City" Operate? Leveraging Synergies. Washington D.C, Integrated Corridor Management and the Smart Cities Revolution.

Ghiasi, A., Hussain, O., Qian, Z.S., Li, X., 2017. A mixed traffic capacity analysis and lane management model for connected automated vehicles: A Markov chain method. Transportation Research Part B: Methodological 106, 266–292. https://doi.org/10.1016/J.TRB.2017.09.022.

Ghiasi, A., Hussain, O., Qian, Z.S., Li, X., 2020. "Shaw" Lane Management with Variable Lane Width and Model Calibration for Connected Automated Vehicles. J Transp Eng A Syst 146, 04019075. https://doi.org/10.1061/JTEPBS.0000283.

Gkartzonikas, C., Gkritza, K., 2019. What Have We Learned? A Review of Stated Preference and Choice Studies on Autonomous Vehicles. Transp Res Part C Emerg Technol 98, 323–337. https://doi.org/10.1016/j.trc.2018.12.003.

Gurman, M., 2021. Apple Accelerates Work on Car Project, Aiming for Fully Autonomous Vehicle [WWW Document]. accessed 12.10.21 Bloomberg. https://www.bloomberg.com/news/articles/2021-11-18/apple-accelerates-work-on-car-aims-for-fully-autonomous-vehicle.

Hendrickson, C.T., Lave, L.B., Matthews, H.S., 2006. Environmental life cycle assessment of goods and services : an input-output approach. Routledge, Oxfordshire, UK.

Jeon, C.M., Amekudzi, A., 2005. Addressing Sustainability in Transportation Systems: Definitions, Indicators, and Metrics. Journal of Infrastructure Systems 11, 31–50. https://doi.org/10.1061/(ASCE)1076-0342(2005)11:1(31).

Jorgensen, K., 2008. Technologies for electric, hybrid and hydrogen vehicles: Electricity from renewable energy sources in transport. Util Policy 16, 72–79. https://doi.org/10.1016/J.JUP.2007.11.005.

Labi, S., 2014. Introduction to Civil Engineering Systems: A Systems Perspective to the Development of Civil Engineering Facilities. John Wiley & Sons Inc, Hoboken, New Jersey.

Lavasani, M., Jin, X., Du, Y., 2016. Market Penetration Model for Autonomous Vehicles on the Basis of Earlier Technology Adoption Experience. Transp Res Rec 2597, 67–74. https://doi.org/10.3141/2597-09.

Le Hong, Z., Zimmerman, N., 2021. Air quality and greenhouse gas implications of autonomous vehicles in Vancouver. Canada. Transp Res D Transp Environ 90, 102676. https://doi.org/10.1016/J.TRD.2020.102676.

Li, C., Cao, Y., Zhang, M., Wang, J., Liu, J., Shi, H., Geng, Y., 2015. Hidden Benefits of Electric Vehicles for Addressing Climate Change. Scientific Reports 2015 5:1 5, 1–4. 10.1038/srep09213.

Li, Q., Li, X., 2022. Trajectory planning for autonomous modular vehicle docking and autonomous vehicle platooning operations. Transp Res E Logist Transp Rev 166, 102886. https://doi.org/10.1016/J.TRE.2022.102886.

Li, Q., Yao, H., 2022. Individual variable speed limit trajectory planning considering stochastic arriving patterns. Int J Coal Sci Technol 9, 1–17. https://doi.org/10.1007/S40789-022-00543-8/FIGURES/9.

Liu, C., Du, Y., Wong, S.C., Chang, G., Jiang, S., 2020. Eco-based Pavement Lifecycle Maintenance Scheduling Optimization for Equilibrated Networks. Transp Res D Transp Environ 86, 102471. https://doi.org/10.1016/J.TRD.2020.102471.

Liu, Z., Song, Z., 2019. Strategic Planning of Dedicated Autonomous Vehicle Lanes and Autonomous Vehicle/toll Lanes in Transportation Networks. Transp Res Part C Emerg Technol 106, 381–403. https://doi.org/10.1016/j.trc.2019.07.022.

Lou, Y., Yin, Y., Lawphongpanich, S., 2009. Robust Approach to Discrete Network Designs with Demand Uncertainty. Transportation Research Record: Journal of the Transportation Research Board 86–94. https://doi.org/10.3141/2090-10.

Ma, R., Ban, X.J., Szeto, W.Y., 2017. Emission Modeling and Pricing on Single-destination Dynamic Traffic Networks. Transportation Research Part B: Methodological 100, 255–283. https://doi.org/10.1016/j.trb.2017.02.007.

Ma, R., Ban, X., Szeto, W.Y., 2015. Emission Modeling and Pricing in Dynamic Traffic Networks, in: Transportation Research Procedia. Elsevier, pp. 106–129. 10.1016/j.trpro.2015.07.007.

Madadi, B., van Nes, R., Snelder, M., van Arem, B., 2020. A Bi-level Model to Optimize Road Networks for a Mixture of Manual and Automated Driving: An Evolutionary Local Search Algorithm. Computer-Aided Civil and Infrastructure Engineering 35, 80–96. https://doi.org/10.1111/mice.12498.
Miralinaghi, M., 2018. Multi-period tradable credit schemes for transportation and environmental applications. Purdue University.
Miralinaghi, M., Peeta, S., 2019. Promoting Zero-emissions Vehicles Using Robust Multi-period Tradable Credit Scheme. Transp Res D Transp Environ 75, 265–285. https://doi.org/10.1016/j.trd.2019.08.012.
Miralinaghi, M., Peeta, S., He, X., Ukkusuri, S.V., 2019. Managing morning commute congestion with a tradable credit scheme under commuter heterogeneity and market loss aversion behavior. Transportmetrica B 7. https://doi.org/10.1080/21680566.2019.1698379.
Miralinaghi, M., Peeta, S., 2020. Design of a Multiperiod Tradable Credit Scheme under Vehicular Emissions Caps and Traveler Heterogeneity in Future Credit Price Perception. Journal of Infrastructure Systems 26, 04020030. https://doi.org/10.1061/(asce)is.1943-555x.0000570.
Ong, G.P., Hwang, Y.H., 2019. A Concept for a Smart, Cool and Naturalistic Active Mobility Infrastructure Landscape for Singapore. In: In: 2019 International Conference on Smart Cities, pp. 16–20.
Park, S.Y., Kim, J.W., Lee, D.H., 2011. Development of a Market Penetration Forecasting Model for Hydrogen Fuel Cell Vehicles considering Infrastructure and Cost Reduction Effects. Energy Policy 39, 3307–3315. https://doi.org/10.1016/J.ENPOL.2011.03.021.
Peters, D.R., Schnell, J.L., Kinney, P.L., Naik, V., Horton, D.E., 2020. Public Health and Climate Benefits and Trade-Offs of U.S. e2020GH000275 Vehicle Electrification. Geohealth 4. https://doi.org/10.1029/2020GH000275.
Pourgholamali, M., Miralinaghi, M., Ha, P.Y.J., Seilabi, E.S., Labi, S., 2023. Sustainable Deployment of Autonomous Vehicles Dedicated Lanes in Urban Traffic Networks. SSRN Electronic Journal. https://doi.org/10.2139/SSRN.4406881.
Pribyl, O., Blokpoel, R., Matowicki, M., 2020. Addressing EU Climate Targets: Reducing CO2 Emissions using Cooperative and Automated Vehicles. Transp Res D Transp Environ 86, 102437. https://doi.org/10.1016/J.TRD.2020.102437.
Pudāne, B., Correia, G., 2020. On the impact of vehicle automation on the value of travel time while performing work and leisure activities in a car: Theoretical insights and results from a stated preference survey – A comment. Transp Res Part A Policy Pract 132, 324–328. https://doi.org/10.1016/j.tra.2019.11.019.
Raghunathan, A.U., Biegler, L.T., 2012. An Interior Point Method for Mathematical Programs with Complementarity Constraints (MPCCs). 15, 720–750. https://doi.org/10.1137/S1052623403429081.
Saeed, T.U., Alabi, B.N.T., Labi, S., 2021. Preparing Road Infrastructure to Accommodate Connected and Automated Vehicles: System-Level Perspective. Journal of Infrastructure Systems 27, 06020003. https://doi.org/10.1061/(ASCE)IS.1943-555X.0000593.
Scholtes, S., Stöhr, M., 1999. Exact Penalization of Mathematical Programs with Equilibrium Constraints. SIAM J Control Optim 37, 617–652. https://doi.org/10.1137/S0363012996306121.
Seilabi, S.E., Tabesh, M.T., Davatgari, A., Miralinaghi, M., Labi, S., 2020. Promoting Autonomous Vehicles Using Travel Demand and Lane Management Strategies. Front Built Environ 6, 560116. https://doi.org/10.3389/fbuil.2020.560116.
Seilabi, S.E., Pourgholamali Davarani, M., Miralinaghi, M., He, S.X., Labi, S., 2022. Managing Dedicated Lanes for Connected and Autonomous Vehicles to Address Bottleneck Congestion Considering Morning Peak Commuter Departure Choices. SSRN Electronic Journal. https://doi.org/10.2139/SSRN.4142516.
Shabanpour, R., Mousavi, S.N.D., Golshani, N., Auld, J., Mohammadian, A., 2017. Consumer preferences of electric and automated vehicles. In: 5th IEEE International Conference on Models and Technologies for Intelligent Transportation Systems. https://doi.org/10.1109/MTITS.2017.8005606.
Shabanpour, R., Golshani, N., Shamshiripour, A., Mohammadian, A.K., 2018. Eliciting preferences for adoption of fully automated vehicles using best-worst analysis. Transp Res Part C Emerg Technol 93, 463–478. https://doi.org/10.1016/j.trc.2018.06.014.
Song, Z., He, Y., Zhang, L., 2017. Integrated Planning of Park-and-Ride Facilities and Transit Service. Transp Res Part C Emerg Technol 74, 182–195. https://doi.org/10.1016/j.trc.2016.11.017.
Tesla, 2021. Electric Cars, Solar & Clean Energy [WWW Document]. URL https://www.tesla.com/.
United Nations World Urbanization Prospects: The 2018 Revision 2018 New York, NY.
USDOT Center for Climate Change Congestion Mitigation and Air Quality (CMAQ) Improvement Program 2017 Washington DC.
Valdes-Dapena, P., 2018. Waymo and Jaguar Unveil a Self-driving, Electric SUV [WWW Document]. accessed 12.10.21 CNN. https://money.cnn.com/2018/03/27/technology/waymo-driverless-jaguar-i-pace/index.html.
Wadud, Z., MacKenzie, D., Leiby, P., 2016. Help or Hindrance? The Travel, Energy and Carbon Impacts of Highly Automated Vehicles. Transp Res Part A Policy Pract 86, 1–18. https://doi.org/10.1016/J.TRA.2015.12.001.
Wallace, C.E., Courage, K.G., Hadi, M.A., Gan, A.G., 1998. TRANSYT-7F User's Guide. University of Florida, Gainesville, FL.
Wang, S., De Almeida, H., Correia, G., Lin, H.X., 2022. Assessing the Potential of the Strategic Formation of Urban Platoons for Shared Automated Vehicle Fleets. J Adv Transp 2022. https://doi.org/10.1155/2022/1005979.
Wu, W., Zhang, F., Liu, W., Lodewijks, G., 2020. Modelling the Traffic in a Mixed Network with Autonomous-Driving Expressways and Non-autonomous Local Streets. Transp Res E Logist Transp Rev 134, 101855. https://doi.org/10.1016/j.tre.2020.101855.
Xu, X., Chen, A., Cheng, L., 2015. Reformulating Environmentally Constrained Traffic Equilibrium via a Smooth Gap Function. https://doi.org/10.1080/15568318.2013.777261.
Yang, X., Jeff Ban, X., Ma, R., 2017. Mixed Equilibria with Common Constraints on Transportation. Networks 17, 547–579. https://doi.org/10.1007/s11067-016-9335-9.
Yang, Y., Yin, Y., Lu, H., 2014. Designing Emission Charging Schemes for Transportation Conformity. J Adv Transp 48, 766–781. https://doi.org/10.1002/atr.1226.
Yao, H., Li, X., 2020. Decentralized control of connected automated vehicle trajectories in mixed traffic at an isolated signalized intersection. Transp Res Part C Emerg Technol 121, 102846. https://doi.org/10.1016/J.TRC.2020.102846.
Ye, Y., Wang, H., 2018. Optimal Design of Transportation Networks with Automated Vehicle Links and Congestion Pricing. J Adv Transp. https://doi.org/10.1155/2018/3435720.
L. Zhang S. Lawphongpanich Y. Yin 2009. An active-set Algorithm for Discrete Network Design Problems, in: William, H.K.L., Wong, S.C., Hong, K. Lo (Eds.), Transportation and Traffic Theory, Golden Jubilee 2009 Springer New York 283 300.